

# **Topological phase transition in three dimensional materials**

**Thesis Submitted  
In Partial Fulfilment of the Requirements for the  
Degree of**

**MASTER OF SCIENCE**

**in  
Applied Physics**

**by  
Nidhi  
(2K22/MSCPHY/30)**

**Under the Supervision of  
Dr. Mukhtiyar Singh  
Assistant Professor, Department of Applied Physics  
DELHI TECHNOLOGICAL UNIVERSITY**



**To the  
Department of Applied Physics  
DELHI TECHNOLOGICAL UNIVERSITY  
(Formerly Delhi College of Engineering)  
Shahbad Daultapur, Main Bawana Road, Delhi-110042, India  
May, 2024**



# DELHI TECHNOLOGICAL UNIVERSITY

(Formerly Delhi College of Engineering)  
Shahbad Daultapur, Main Bawana Road, Delhi-42

## CANDIDATE DECLARATION

I **Nidhi** (2K22/MSCPHY/30) hereby certify that the work being presented in the thesis entitled “**Topological phase transition in three dimensional materials**” in partial fulfillment of the requirements for the award of the Degree of Master of Science submitted in the Department of Applied Physics, Delhi Technological University in an authentic record of my work carried out during the period from August 2022 to May 2024 under the supervision of Dr. Mukhtiyar Singh.

The matter presented in the thesis has not been submitted by me for the award of any other degree of this or any other Institute.

Candidate’s Signature

This is to certify that the student has incorporated all the corrections suggested by the examiner in the thesis and that the statement made by the candidate is correct to the best of our knowledge.

Signature of Supervisor



# **DELHI TECHNOLOGICAL UNIVERSITY**

(Formerly Delhi College of Engineering)  
Shahbad Daultapur, Main Bawana Road, Delhi-42

## **CERTIFICATE BY THE SUPERVISOR**

Certified that **Nidhi** (Roll no 2K22/MSCPHY/30) has carried out her project work presented in this thesis entitled “**Topological phase transition in three dimensional materials**” for the award of **Master of Science** from the Department of Applied Physics, Delhi Technological University, Delhi under my supervision. The thesis embodies results of original work, and studies are carried out by the student herself and the contents of the thesis do not form the basis for the award of any other degree to the candidate or to anybody else from this or any other University/Institution.

**Dr. Mukhtiyar Singh**

Assistant Professor,  
Department of Applied Physics,  
DTU-Delhi, India

Date:

## LIST OF CONFERENCES

**Name of Conference:** Recent Advances in Functional Materials (RAFM-2024)

**Conference Dates:** 2024, March 14-16

**Mode of the conference:** online

**Title of the presentation:** *A first-principles* study of strain-driven, structural, dynamical, and topological properties of novel Sn-based ternary chalcogenide SnPbSe<sub>2</sub>

**Venue:** ATMA RAM SANATAN DHARMA COLLEGE, NEW DELHI

**Name of Conference:** International Conference on Materials Genome-III

**Conference Dates:** 2024, February 22-24

**Mode of the conference:** offline

**Title of the poster:** *A first-principles* study of topological phase in Zintl compound KCd<sub>4</sub>As<sub>3</sub>

**Venue:** SRM UNIVERSITY, ANDHRA PRADESH

**Name of Conference:** International Conference on Advanced Functional Materials and Devices (AFMD-2024)


**Conference Dates:** 2024, February 26-29

**Mode of the conference:** online

**Title of the poster:** *A first-principles* study of topological phase in Zintl compound KCd<sub>4</sub>As<sub>3</sub>

**Venue:** SRM UNIVERSITY, Kttankulathur, Tamil Nadu

## PARTICIPATION RECORD



### ATMA RAM SANATAN DHARMA COLLEGE


#### UNIVERSITY OF DELHI

Accredited Grade 'A++' By NAAC || All India 6th Rank in NIRF (Ministry of Education)

2nd International Conference on

### Recent Advances in Functional Materials (RAFM-2024)

Under the aegis of IQAC and DBT (GoI) star college scheme



## Certificate of Oral Presentation

This is to certify that Prof./Dr./Mr./Ms.


**NIDHI**

Delhi Technological University, New Delhi

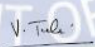
has presented his/her research work as oral presentation titled

**A first-principles investigation of strain-driven structural, dynamical, and topological properties of novel Sn-based ternary chalcogenide**

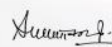
in 2nd International Conference on "Recent Advances in Functional Materials" (RAFM-2024) organised by Department of Physics under the aegis of IQAC ARSD College, University of Delhi & DBT (GoI) Star College during March 14-16, 2024 via online mode.



**Dr. Manish Kumar**  
Convener, RAFM-2024



**Prof. Vinita Tuli**  
Coordinator, IQAC



**Prof. Gyantosh Kumar Jha**  
Principal, ARSD College

Certificate No: ARSD/RAFM-2024/OT/114



International Conference on

### Advanced Functional Materials and Devices

(AFMD-2024)

## Certificate of Participation



This is to certify that

**Ms. Nidhi Kadyan**

Delhi Technological University

has presented the work, entitled

**A first-principles study of the topological phase in zintl compound  $KCd_2As$ ,**

in the International Conference on Advanced Functional Materials and Devices (AFMD-2024) organized by Nanotechnology Research Centre (NRC), SRM Institute of Science and Technology, Kattankulathur, Tamil Nadu, India, held during February 26-29, 2024.



**Dean Sciences**  
SRMIST



**Convener**  
AFMD - 2024, SRMIST



**Co-Convener**  
AFMD - 2024, SRMIST



## International Conference on Materials Genome -III

### ICMG - III

### *Certificate of Participation*

This is to certify that

**Nidhi**

has attended and presented a poster titled

**A first-principles study of the topological phase in Zintl compound  $KCd_4As_3$**

in the *International Conference on Materials Genome-III* held at SRM University AP, Andhra Pradesh, India from 22<sup>nd</sup> to 24<sup>th</sup> February, 2024 .

Chairperson  
Prof. Yoshiyuki Kawazoe  
Tohoku University, Japan

Convener  
Prof. Ranjit Thapa  
SRM University-AP, India

sponsored by



# COPYRIGHT FORM

## Licence to Publish Proceedings Papers

**SPRINGER NATURE**

---

Licensee	Springer Nature Singapore Pte Ltd.	(the 'Licensee')
Title of the Proceedings Volume/Edited Book or Conference Name:	Recent Advances in Functional Materials, Volume 1 - Select Proceedings of RAFM 2024	(the 'Volume')
Volume Editor(s) Name(s):	Dr. Manish Kumar, Dr. Anjani Kumar Singh, Dr. Subhash Sharma, Prof. Devendra Kumar	
Proposed Title of the Contribution:	A first-principle study of strain driven structural, dynamical and topological properties of novel Sn-based ternary chalcogenide SnPbSe <sub>2</sub>	(the 'Contribution')
Series: The Contribution may be published in the following series	A Springer book series Springer Proceedings in Materials	
Author(s) Full Name(s):	Nidhi, Ramesh Kumar, Mukhtiyar Singh	(the 'Author')
<i>When Author is more than one person the expression "Author" as used in this Agreement will apply collectively unless otherwise indicated.</i>		
Corresponding Author Name:	Mukhtiyar Singh	
Instructions for Authors	<a href="https://www.springer.com/go/authors-editors/conference-proceedings/conference-proceedings-guidelines">https://www.springer.com/go/authors-editors/conference-proceedings/conference-proceedings-guidelines</a>	(the 'Instructions for Authors')

## COMMUNICATION RECORD



Dr. Mukhtiyar Singh <mukhtiyarsingh@dtu.ac.in>

---

### Decision Letter (RAFM\_32)

1 message

---

RAFM-2024, Department of Physics ARSD College <rafm@arsd.du.ac.in>  
To: mukhtiyarsingh@dtu.ac.in

Wed, Jun 5, 2024 at 9:05 PM

Ms. Ref. No.: RAFM\_32

Title: A first-principles study of strain-driven structural, dynamical, and topological properties of novel Sn-based ternary chalcogenide SnPbSe<sub>2</sub>

Dear Mr. Mukhtiyar Singh

I am pleased to inform you that your paper " A first-principles study of strain-driven structural, dynamical, and topological properties of novel Sn-based ternary chalcogenide SnPbSe<sub>2</sub> "**Select Springer Nature Proceedings of RAFM 2024 (Scopus Indexed)**".

**Regards**

**Editor, RAFM-2024**



## ABSTRACT

In the present work, our first-principles study shows the topological phase transition in rare-earth monpnictides GdSb and ternary chalcogenide SnPbSe<sub>2</sub> under the influence of hydrostatic pressure and biaxial strain. The dynamical and thermodynamical stabilities of materials are verified with the applied hydrostatic pressure and biaxial strain. The structural, electronic, and topological properties are studied using the density functional theory with hybrid functionals. The topological nature has been verified by calculating  $Z_2$  topological invariants and surface density of states (SDOS). At ambient conditions, both materials show a topological trivial nature, which has been verified by the energy band gap in the bulk band structure and (0;000) values of  $Z_2$  topological invariants. The topological phase transition in GdSb and SnPbSe<sub>2</sub> is obtained at 6 GPa of hydrostatic pressure and 2% of biaxial strain respectively. The occurrence of inverted contribution of orbitals in band inversions near the Fermi level are observed. The non-zero value of first  $Z_2$  topological invariant and presence of Dirac cone in the surface state has verified the non-trivial topological nature of materials. However, when we further increase the hydrostatic pressure and biaxial strain in these materials, respectively, another band inversion in bulk band structure is also observed. The calculation of  $Z_2$  topological invariants is (0;000) and has verified the trivial nature of materials after even number of band inversions.

## ACKNOWLEDGEMENTS

I would like to express my deep appreciation to **Dr. Mukhtiyar Singh**, Assistant Professor at the Department of Applied Physics, Delhi Technological University, for his invaluable guidance and unwavering encouragement throughout this research. His vast knowledge, motivation, expertise, and insightful feedback have been instrumental in every aspect of preparing this research plan.

I am also grateful to **Prof. A.S. Rao**, Head of the Department, for his valuable insights, suggestions, and meticulous evaluation of my research work. His expertise and scholarly guidance have significantly enhanced the quality of this thesis.

I am also very grateful to **Mr. Ramesh Kumar**, Senior Research Fellow, Department of Applied Physics at Delhi Technological University's Department of Applied Physics, for his guidance and for sharing his knowledge and experience in this area. I appreciate his unwavering advice and assistance.

I would also like to thank research scholars **Dr. Rajesh Kumar**, **Ms. Sangeeta**, **Mr. Kulwinder Kumar** in *CQMD* Lab and my friends **Mr. Stephen Shaiju Mathew**, **Ms. Aarti Rajput** and **Ms. Neha Vashisht** for their continuous support and understanding. I am also thankful to my family and colleagues for their invaluable support, care, and patience during this project.

My heartfelt thanks go out to the esteemed faculty members of the Department of Applied Physics at Delhi Technological University. I extend my gratitude to my family for their unwavering support and encouragement during this challenging journey. Their intellectual exchanges, constructive critiques, and camaraderie have enriched my research experience and made it truly fulfilling.

We also want to acknowledge National Supercomputing Mission (NSM) for providing computing resources of 'PARAM Siddhi-AI', under the National PARAM Supercomputing Facility (NPSF), C-DAC, Pune and supported by the Ministry of Electronics and Information Technology (MeitY) and Department of Science and Technology (DST), Government of India.

**Nidhi**  
**(2K22/MSCPHY/30)**

## TABLE OF CONTENT

Candidate's Declaration .....	i
Certificate .....	ii
List of Conferences.....	iii
Participation Record.....	iv
Copyright Form.....	vi
Communication Record.....	vii
Abstract .....	viii
Acknowledgments .....	ix
Table of Content.....	x
List of Tables.....	xii
List of Figures.....	xiii
List of symbols, Abbreviations.....	xv
Chapter 1 Introduction .....	30
1.1 Quantum Hall Effect.....	19
1.1.2 Quantum Spin Hall State and Topological Insulators.....	20
1.1.3 Topology.....	21
1.1.4 Band inversion in Topological Insulators.....	22
1.1.5 Time Reversal Symmetry.....	23
1.1.6 Combine effect of space and Time Reversal Symmetry .....	23
1.2 Literature Survey.....	24
1.2.1 Topological Semimetals.....	25
1.2.2 Ternary Chalcogenide family.....	26
1.2.3 Strain and Pressure induced Topological Phase Transition.....	28
1.2.4 Topological Phase Transition in TlBiS <sub>2</sub> and TlSbS <sub>2</sub> using strain and Hydrostatic pressure.....	29
1.2.3 Pressure induce Topological Phase Transition in rare-earth monopnictides family.....	30
Chapter 2 Methodology.....	31-39
2.1 Many body problem.....	31
2.2 Density Functional Theory.....	33

2.3 Exchange correlational functional .....	34
2.4 Generalized Gradient approximation .....	35
2.5 Perdew – Burke – Ernzerhof (PBE).....	36
2.6 Modified Becke – Johnson (mBJ).....	36
2.7 Hybrid – Scuseria-Ernzerhof (HSE).....	36
2.8 Energy Cut Off.....	37
2.9 k-mesh sampling.....	37
2.10 $Z_2$ Topological Invariants.....	38
2.11 Parity.....	38
2.12 VASP.....	39
2.13 Phonopy Package.....	39
2.14 Wannier 90Packages.....	39
Chapter 3 The TPT in rare earth monpnictides.....	40-47
3.1 Abstarct.....	40
3.2 Computational Details.....	41
3.3 Results and Discussions.....	45
3.4 $Z_2$ Topological Invariants.....	46
3.5 Conclusion.....	47
Chapter 4 A <i>first-principles</i> study of strain-driven structural, dynamical, and topological properties of novel Sn-based ternary chalcogenide SnPbSe <sub>2</sub> .....	48-53
4.1 Abstract.....	48
4.2 Computational Details.....	48
4.3 Results and Discussions.....	52
4.4 $Z_2$ Topological Invariants.....	53
References.....	58
Plagiarism verification.....	59

## **LIST OF TABLES**

### **CHAPTER 3**

Table 3.1 parities at all TRIM points in BZ at various pressure ranges of GdSb.

### **CHAPTER 4**

Table 3.1 the product of parities of all valance bands at TRIM points and  $Z_2$  invariants under conditions of SnPbSe<sub>2</sub>.

## LIST OF FIGURES

- Fig. 1.1. (a) Hall set-up (b) Resistance w.r.t. applied magnetic field as observed in Classical Hall Effect.
- Fig. 1.2. (a) The measured low-temperature resistance w.r.t applied magnetic field and (b) Schematic of bulk and edge behaviour of electrons in Quantum Hall Effect.
- Fig. 1.3. (a) Spin-less Quantum Hall bar and (b) its corresponding band structure.
- Fig. 1.4. (a) Spin-full Quantum Spin-Hall bar and (b) its corresponding band structure.
- Fig.1.5. Doughnut ( $g = 0$ ) can be transformed into coffee mug ( $g = 1$ ) and trefoil wire ( $g = 2$ ) are topological equivalent
- Fig.1.6. (a) Energy w.r.t adiabatic deformation for a quantum system (b) Topological equivalence in terms of bands.
- Fig.1.7. (a) Weyl node (b) Dirac node (c) Nodal line.
- Fig.1.8. Schematic diagram of Band structure at different hydrostatic pressure.
- Fig. 1.9. band structure of  $\text{TiSbS}_2$  at (a) 0 GPa (b) 2 GPa (c) 3GPa (d) 5GPa (e) 8 GPa hydrostatic pressure.
- Fig. 1.10. Band structure of YbAs at (a) ambient pressure (b) at 6 GPa hydrostatic pressure.
- Fig.2.1. Represents the theme of Density functional theory.
- Fig.3.1. (a) Crystal structure of GdSb (a) NaCl-type (b) CsCl- type (c) The Brillion zone of GdSb. The shaded area (green color) is representing the projection of the bulk Brillion zone on the ( $\Gamma$ ) surface Brillion zone (SBZ), with symmetry points in the SBZ displayed (red color).
- Fig.3.2. (a) Enthalpy of GdSb as function of pressure for NaCl-type to CsCl-type structure. (b) Variation in relative volume of GdSb as a function of pressure. The phonon dispersion of GdSb at (c) 0 GPa, (d) 26.1 GPa.
- Fig. 3.3. The band structure of GdSb with inclusion of SOC effect using (a) GGA-PBE, (b) Projected density of states (c) HSE06 (d) The surface state. The Fermi level is set to 0 eV.
- Fig. 3.4 (a) Band structure of GdSb with the inclusion of SOC effect using HSE06 functional at 6 GPa (b) The surface state. The Fermi level is set to be 0 eV.
- Fig. 3.5 (a) Band structure of GdSb with the inclusion of SOC effect using HSE06 functional at 12 GPa. (b, c) the surface state. The Fermi level is set to be 0 eV.

Fig.4.1. The crystal structure of SnPbSe<sub>2</sub> in (a) conventional unit cell (b) primitive unit cell. The phonon dispersion spectrums of SnPbSe<sub>2</sub> (c) at ambient condition and (d-e) applied 2% of uniaxial and biaxial strain.

Fig.4.2. The electronic band structure of SnPbSe<sub>2</sub> at ambient condition using (a) PBE+SOC and (b) mBJ+SOC functionals. The Fermi energy is set to 0 eV.

Fig.4.3. The electronic band structure of SnPbSe<sub>2</sub> using TB-mBJ functional (a) at 2% biaxial strain (b) at 3% biaxial strain. The Fermi energy is set to 0 eV.

Fig.4.4. The first Z<sub>2</sub> topological invariant ( $\nu_0$ ) as a function of applied biaxial strain.

## LIST OF SYMBOLS AND ABBREVIATIONS

S. No.	Symbol	Full Form
1	QHE	Quantum Hall Effect
2	M.F.	Magnetic Field
3	TRS	Time Reversal Symmetry
4	QSH	Quantum Spin Hall
5	BZ	Brillion Zone
6	TIs	Topological Insulators
7	DFT	Density Functional Theory
8	PBE	Perdew-Burke-Ernzerhof
9	HSE	Heyd-Scuderia-Ernzerhof
10	DOS	Density of States
11	GGA	Generalised Gradient Approximations
12	PDOS	Projected Density of States
13	$E_g$	Band-Gap
14	Å	Angstrom
15	eV	electron-volt
16	ARPES	Angle Resolved Photoemission Spectroscopy
17	SOC	Spin-orbit Coupling
18	$\Gamma$	Gamma
19	SS	Surface State
20	TB-mBJ	Tran Blaha modified Becke Johnson
21	LAPW	Linear augmented plane wave
22	VB	Valence Band
23	CB	Conduction Band
24	vdW	van-der Wall
25	vdW	van-der Wall
26	TRIM	Time Reversal Invariant Momenta
27	TQPT	Topological Quantum Phase Transition



# CHAPTER 1

## INTRODUCTION

Traditionally, the phase transition in solids and liquids in the view of condensed matter physics are associated with the change in temperature or pressure. The understanding of phases of matter is associated with the process of broken symmetries and this type of phase transition occurs with the classical phenomena [1]. On the other hand the quantum phase transition phenomena occur at the low temperature and quite difficult to observe e.g. the transition of paramagnetic phase to ferromagnetic phase belongs to quantum regime.

### 1.1.1 Quantum Hall Effect

K. Von Klitzing in 1980 discovered the Quantum Hall Effect (QHE), had a great impact on condensed matter physics that is not based the conventional idea of broken symmetry [2]. According to the phenomena of classical hall effect if there is a material placed in an electric field x-direction and if we apply external M.F. along z-direction then according to Lorentz force a finite voltage ‘ $V_H$ ’ is induced in the y-direction as shown in Fig. 1.1(a). The measured transverse resistance ( $R_{xy}$ ) is given by

$$R_{xy} = \frac{V_y}{I_x} = \frac{E_y}{J_x} \quad 1.1$$

The resistance ( $R_{xx}$ ) can be obtained by measuring the longitudinal resistivity and dividing it by appropriate lengths. The plot of resistance w.r.t magnetic field is shown in Fig. 1.1(b).

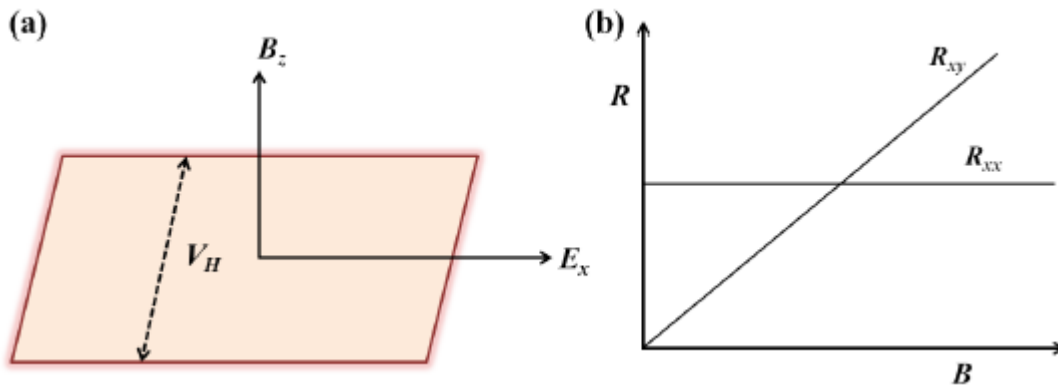


Fig. 1.1. (a) Hall set-up (b) Resistance w.r.t. applied magnetic field as observed in Classical Hall Effect. [2]

In the presence of strong M.F. and at low temperatures and these classical phenomena fails and the quantum effects are dominating as shown by resistance plot versus magnetic field in Fig 1.2 (a). K. Von Klitzing in 1980 discovers the phenomena of Quantum Hall Effect and got Nobel prize in 1985 [2]. From Fig 1.2 (a) the hall resistance  $R_{xy}$  shows plateaus on varying the M.F. and these plateaus are robust to impurities present in the sample. Here, transverse resistance  $R_{xy}$  known as Hall resistance show plateaus on varying the M.F., which takes the value

$$R_{xy} = \frac{h}{e^2} \frac{1}{\nu} \quad \nu \in \mathbb{Z} \quad 1.2$$

Where  $\nu$  is experimentally observed accurate up to  $10^{-9}$  decimal places and is independent of the geometry of the sample [3]. The longitudinal resistance  $R_{xx}$  also shows the interesting behaviour as the form of plateau. The value of  $R_{xx} = 0$  remains as the  $R_{xy}$  rests on the plateau and spikes when  $R_{xy}$  jumps from one to another. It can be said that when  $R_{xx} = 0$  the system is a perfect conductor and the sudden change in  $R_{xx}$  indicating there is resistance that the system undergoes a phase transition from metal to insulator. For the understanding of such transition, we consider the behaviour of electrons in the bulk as well as surface in the presence of M.F. From Fig. 1.2 (b) it can be seen that in the bulk electrons moves in a circular orbit and forms cyclotron which are localized and hence insulating. But, at the boundary the electrons collide and bounced back which forms the skipping orbits, made them to move in one direction and hence conducting.

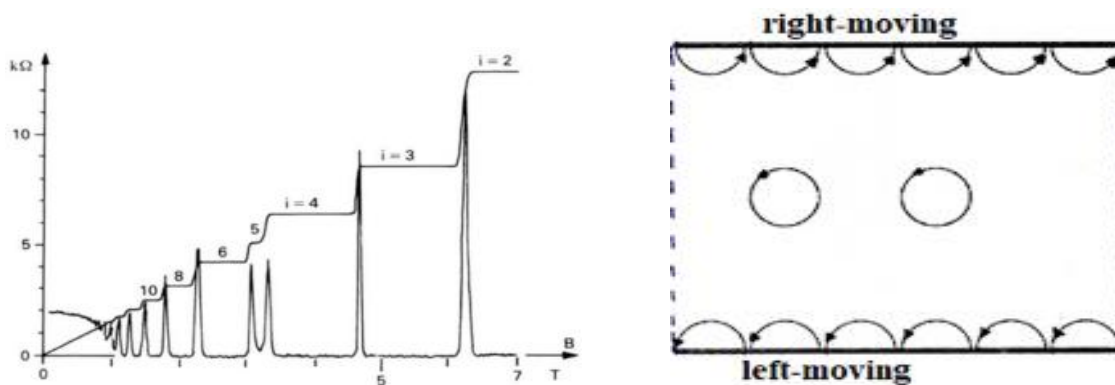


Fig. 1.2. (a) The measured low-temperature resistance w.r.t applied magnetic field and (b) Schematic of bulk and edge behaviour of electrons in Quantum Hall Effect. [3]

For a fixed direction of M.F., motion of electrons at two edges will be in opposite direction, known as Chiral edges and exhibit a special feature as they are robust to any kind of perturbation as shown in Fig. 1.3. The M.F. break the time reversal symmetry (TRS).

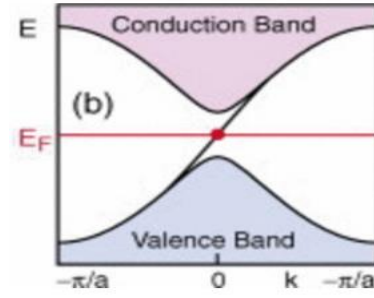
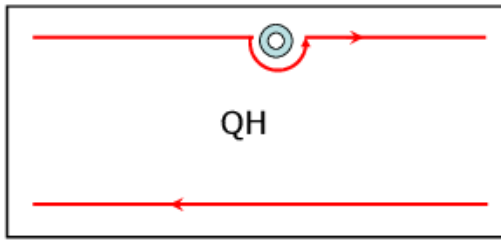


Fig. 1.3. (a) Spin-less Quantum Hall bar and (b) its corresponding band structure. [3]

### 1.1.2 Quantum Spin Hall state and Topological Insulators

The Quantum Spin Hall (QSH) states is another topological class different from the QH because of the external M.F. required in QHE, breaks TRS while QSHE does not require an external M.F and is TR invariant [4]. QSH posses a bulk gap but topologically protected gapless edge states having a unique helical property of counter-propagating two spin-channels per edge in Fig.1.4. The superposition of two mental copies of QH states for up and down spins, can be considered to form a QSH state.

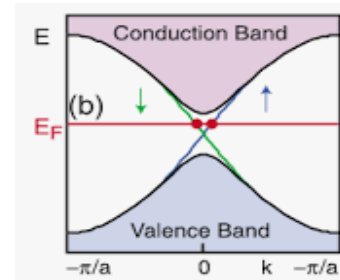
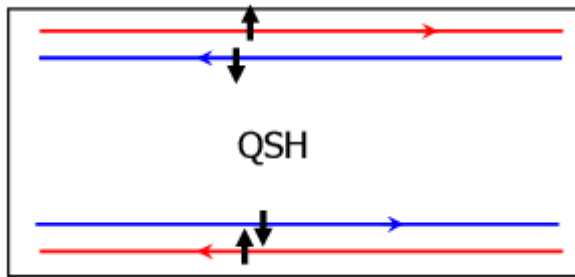


Fig. 1.4. (a) Spin-full Quantum Spin-Hall bar and (b) its corresponding band structure. [5]

In the Brillouin zone (BZ), presence of TRS enforces the energy levels to cross each other. The crossing of energy levels disables a QSH state to continuously deform into a topologically trivial insulator without helical edges, hence distinguishes a topologically different state of matter. This type of state is known as ‘2D Topological Insulator’ (TI) [5]. Bernevig et al. in 2006 predicted it theoretically, for the first time and in 2007, it is experimentally observed by Konig et al. in HgTe/CdTe quantum wells [6]. The major development in the discovery of TIs lie in the fact that QHE cannot be observed in three-dimensions (3D), while QSHE can be generalized to three-dimensional TIs [7]. In 2007, Fu and Kane predicted the first 3D version of TIs by considering a certain range of compositions in  $\text{Bi}_{1-x}\text{Sb}_x$  alloy [8] and in 2008, Hsieh et al. verified the non-trivial surface spectrum by angle-resolved photoemission spectroscopy (ARPES) measurements [9]. Other simpler

versions of 3D TIs were also predicted in  $\text{Bi}_2\text{Te}_3$ ,  $\text{Sb}_2\text{Te}_3$ , and  $\text{Bi}_2\text{Se}_3$ , where a large bulk gap and a solid Dirac cone is observed at the surface [10]. These remarkable features of TIs make them susceptible for potential applications in quantum computing [11] and spintronics [12], thermoelectric materials [13], chemical catalyst [14].

### 1.1.3 Topology:

Topology is a mathematical concept which studies the invariant properties of the geometrical objects under smooth deformations. If the two objects are deformed into each other without creating any holes in it, then the objects are said to be topological equivalent. The distinguishes between two topological classes are done through topological invariant known as ‘genus’ which represent the number of holes in the systems [15].

For example a sphere with  $g = 0$  can be smoothly transformed into a bowl and a doughnut with  $g = 1$  deformed into a coffee cup without creating a hole in it, thus are ‘topologically equivalent’. In others words, we can say that two objects having the same genus can be deformed into one another, and are ‘topological equivalent’.

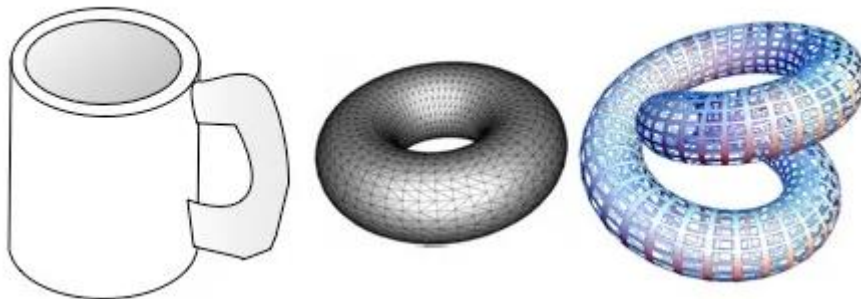


Fig. 1.5. Doughnut ( $g = 1$ ) can be transformed into coffee mug ( $g = 1$ ) and trefoil wire ( $g = 2$ ) are topological equivalent. [16]

### 1.1.4 Band Inversion in Topological Insulators:

The crystalline solids in an electronic structure helps in determining the occupation of electrons in energy band that helps in determining the macroscopic properties of a material such as thermal conductivity and electrical properties of a material. In semiconductor physics the materials are mainly classified into three types according to their band theory. 1) Metals 2) Semiconductor which can be converted into metals by chemical doping and temperature 3) Insulators. The classification of these materials is done with the help of energy gap present between valence and conduction band [17]. Recent discovery in condensed matter physics identified new materials known as TIs. They have insulating in their bulk but possess gapless

metallic surface states. From the band theory in solids geometry includes understanding of topological class of insulators [17]. An insulator is the material where there exists a definite gap between its ground state and all excited states. The thought of topological equivalence for insulators is based on the principle about adiabatic continuity. According to this, a system will stay in its ground state during smooth deformations. In this context, two insulators are considered topologically equivalent if they can be connected to each other without closing the gap between energy states [18]. However, when the gap closes at a quantum critical point, the energy states reverse, leading to a phase transition. Such insulators are then termed topologically in equivalent Fig. 1.6 (a). The transition from a trivial to a non-trivial topological phase is marked by a band inversion. This process signifies a change in the arrangement of energy bands, reflecting a transformation from one topological phase to another Fig. 1.6 (b).

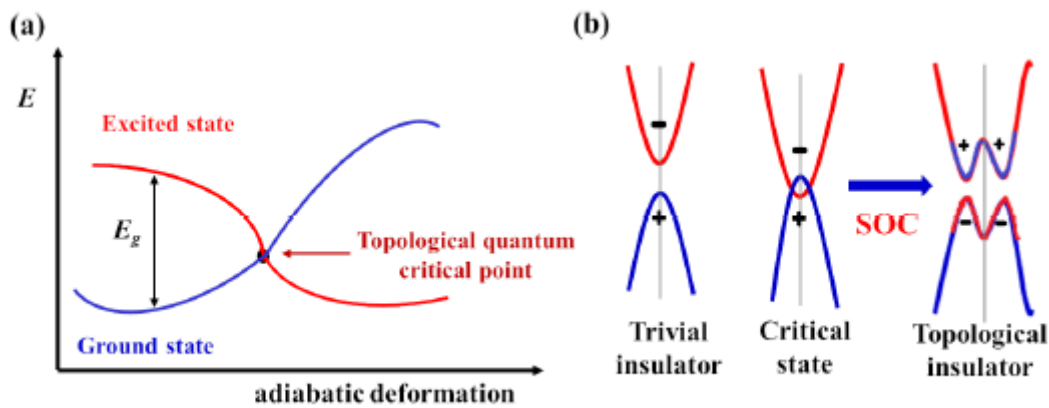


Fig.1.6. (a) Energy w.r.t adiabatic deformation for a quantum system (b) Topological in equivalence in terms of bands. [18]

The appearance of BI is the primary signature of non-trivial topological behaviour of material. Energy gap that closes at the point of conduction band (CB) and valence band (VB); bands are inverted at that point is known as BI. This happens at the high symmetric points in the BZ at some specific points known as Time reversal invariant points (TRIM). The arrangement of energy levels forming the edges of the gap undergoes inversion due to strong Spin-Orbit Coupling (SOC), particularly associated with heavier elements [19-20]. TIs are insulators in their  $d$ -dimensional interior bulk but allows metallic conduction in their  $(d-1)$  dimensional boundaries. The surface states (SS) are protected by time reversal symmetries and robust against small perturbation [21-22]. The SS of these materials contain Dirac cone and energy disperses linearly at these points. The presence of Dirac cone further confirms the

trivial or non trivial nature of system. The odd number of Dirac cone signifies the topological behaviour of material and the even number tells the trivial nature of material. Furthermore, we have also calculated the  $Z_2$  index,  $\nu_0$ , which can be either 0 (depicting a topologically trivial phase) or 1 (indicating a non-trivial phase) according to the Kane and Mele criteria. The overall behaviour of 3D TIs requires a set of four  $Z_2$  numbers:  $(\nu_0; \nu_1\nu_2\nu_3)$ . The indices  $\nu_1$ ,  $\nu_2$ , and  $\nu_3$ , termed weak indices [23]. Consequently, analyzing surface states and determining the  $Z_2$  invariant provides information about the material's topological nature.

### 1.1.5 Time reversal symmetry:

A dynamical variable is considered to have Time-reversal Symmetry (TRS) in Classical Mechanics (C.M.) if it is invariant under the operation  $\mathbf{t} \rightarrow -\mathbf{t}$ . For instance, velocity ( $\mathbf{v}$ ), momentum ( $\mathbf{p}$ ), and magnetic field are time-reversal variant quantities, location ( $\mathbf{x}$ ) and electric field ( $\mathbf{E}$ ) are time-reversal invariant.

However, in Quantum Mechanics (Q.M.), the replacement of  $\mathbf{t} \rightarrow -\mathbf{t}$  doesn't represent the solution of Schrodinger equation

$$i\hbar \frac{d\psi}{dt} = \left(-\frac{\hbar^2}{2m} \Delta^2 + V\right)\psi \quad 1.3$$

It also doesn't satisfy the position-momentum uncertainty relation.

$$[x, p] = i\hbar \quad 1.4$$

$$[x, p] \neq i\hbar \quad 1.5$$

To fulfil equations 1.3 and 1.5, 'i' needs to be changed to '-i'. Note that while there is an uncertainty relation between energy and time in Q.M., there is no operator for time. Time-reversal must therefore be designed in its own context in Q.M., and Wigner proposed that it must be anti-linear and properly referred to as Motion Reversal [24].

### 1.1.6 Combine effect of space inversion and Time inversion symmetry:

In an isolated atom, the crystal having space -inversion symmetry results into:

$$E(\mathbf{k}, \uparrow) = E(-\mathbf{k}, \uparrow) \quad 1.6$$

$$E(\mathbf{k}, \downarrow) = E(-\mathbf{k}, \downarrow) \quad 1.7$$

and TRS results into:

$$E(\mathbf{k}, \uparrow) = E(-\mathbf{k}, \downarrow) \quad 1.8$$

If both equation 1.7 and equation 1.8 are simultaneously satisfied, bands are spin degenerate at the same  $k$ -point.

$$E(\mathbf{k}, \uparrow) = E(\mathbf{k}, \downarrow) \quad 1.9$$

i.e., energy is independent of the electron's spin. Hence, spin-splitting is not permissible in the bulk of the crystals preserving both space-inversion as well as TRS, thus such solids remain spin-degenerate at TR point [25]. Generally speaking, specific locations within the BZ satisfy the inversion symmetry. These high points of symmetry meet equation 1.9. They are referred to as TRIM points for the reasons that follow. The C.B and V.B meet at a specific location on the surface (in  $k$ -space) when the surface bands reduce the gap and have two components corresponding to the spin projections. For both the C.B and V.B, the two components would come together at one of the TRIM points. But the band crossing at TRIM sites is strong and unaffected by non-magnetic perturbations because these points are stable while time symmetry is preserved [26].

## 1.2 Literature Survey

Theoretical progresses generally lead experimental efforts and help predict new phenomena as well as find novel materials in the topological nontrivial matter area. In particular, electronic band theory progress, symmetry indicators and relations of pure topology chemical bonding have been used to predict and classify the topological nature of electronic states in two-dimensional (2D) as well as 3D materials [19]. Through symmetry-driven techniques, high-throughput density functional theory (DFT) computations, catalogued crystallographic symmetry information, and computational searches across topological quantum chemistry, the TL of over 26,000 materials has been investigated. Studies reveal that around 27% of materials are expected to be topologically non-trivial [20]. The estimated large number of topologically non-trivial electronic structures in these computations indicates that many more materials could have existed than what we know from the limited amount of experimentally confirmed examples to date. Interestingly, a few of these compounds have never been synthesized or theorized using the stem methods while some others have been known for decades. New insights have come from interpreting their properties through a topological lens. It is the topological quantum chemistry (and other related approaches), which play an essential role in finding materials by establishing a direct connection between chemical compositions and their topological properties [38]. Future studies aimed at identifying topologically non-trivial materials should use principles of design that extend beyond heuristic and chemical intuition, especially in the area of materials chemistry. This development is in an effort to connect materials as a way enable the material discovery for targeted, optimal property-based behaviour that uses its topological features. A significant

number of 2D and 3D TIs have been predicted by use of ab initio or first-principles calculations [20].  $\text{Bi}_2\text{Se}_3$  [39] and  $\text{Bi}_2\text{Te}_3$  [40] belong to some of the oldest families of 3D TIs, so a lot has been known about their topological states and properties. Because the crystal structures,  $\text{A}_2\text{B}_3$  compounds consist of quintuple layers, which are assembled by weak Van der Waals (vdW) forces, they have natural cleavage planes without breaking strong bonds that bind atoms. The Dirac point of SS in band structure calculation of  $\text{Bi}_2\text{Se}_3$  shows near to Valence Band Maximum (VBM). This gives rise the emergence of electron flow between SS and bulk continuum states at minute separations that destroys the topological transport signature. Consequently, obtaining materials with perfect and well-separated Dirac cones becomes urgent.

### 1.2.1 Topological Semimetals:

The experimentally observation of Weyl semi-metals (WSMs) have shifting the interest from insulating materials to gapless materials after the discovery of TIs. Because of linear band crossing investigating the nontrivial topology in gapless material has gained a great attention in the condensed matter physics [27-29]. These SMs establish many phenomena such as chiral anomaly [30], Weyl fermion quantum transport and magnetoresistance [31-32]. Based on their dimensionality and degeneracy of band crossings topological SMs mainly divided into three types: Weyl, Dirac and nodal-line SMs. Weyl and Dirac SMs characterizes as zero dimensional crossing nodes with two and four fold band degeneracy respectively, while a one dimensional crossings gives the nodal-line SMs. Many studies have predicted the existence of a three-fold degeneracy, which has also been confirmed experimentally [33]. However, one more type of topological SMs has been observed in rare-earth monpnictides, where the not linear band crossings, but posses BI near the Fermi energy [34], which makes their origin topological in nature, similar to TIs. Moreover, triple point fermion (TPF) have been also identified which consists of triply-degenerate nodal point, interconnected with a doubly-degenerate nodal-line, that gives rise to an exotic fermion [35]. The special characteristic of TPF is that, despite Dirac and Weyl fermions, which have a direct analogy to the fermions in the Standard Model, these systems cannot be adequately described by their present topological invariants. Above the all semi-metallic topological states, nodal line SMs is considered as a precursor for other topological phase: convert into Dirac point, can evolved into Weyl points or become TIs by the introduction of the SOC or symmetry breaking [36].



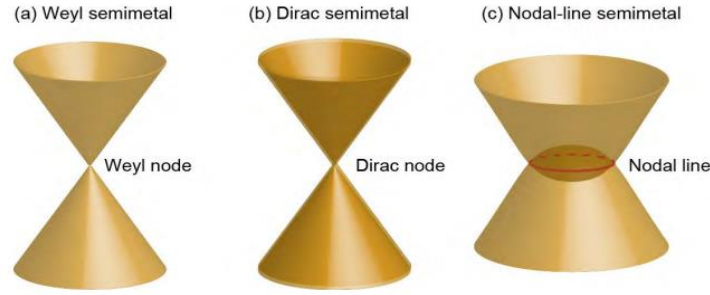


Fig. 1.7. (a) Weyl node (b) Dirac node (c) Nodal line. [37]

### 1.2.2 Ternary Chalcogenide family:

Theoretical calculations suggest that TI-based ternary chalcogenides, like  $\text{TlSbTe}_2$ , exhibit a Dirac-cone SS centered at the  $\Gamma$ -point and are expected to represent a 3D TI phase that is theoretically well isolated from the bulk continuum [41]. The 3D character of TI-based materials originates from the strong coupling between neighbouring atomic layers within each tight binding layer, unlike the typical vdW forces in  $\text{Bi}_2\text{Se}_3$ . The density functional theory (DFT) calculations were conducted in order to probe the electronic structure of a number of TI-based TIs, such as  $\text{TlAB}_2$  ( $A = \text{Bi, Sb}$ ;  $B = \text{S, Te, Se}$ ) and shows non-trivial behaviour. The surface termination plays an important role in  $\text{TlBiSe}_2$  and  $\text{TlBiTe}_2$  [42-43]. After that, the efforts were spent on the isostructural substitution in  $\text{TlBiSe}_2$  material itself to keep its TL properties. In-based compounds such as  $\text{InBiTe}_2$  and  $\text{InSbTe}_2$ , which crystallize in the  $\text{TlBiSe}_2$  like structure; they do not have the Dirac cone like feature and it actually means that they are topologically trivial [41]. These TI-based ternary chalcogenide belongs to a rhombohedral unit cell with space group  $R\bar{3}m$  and contains a primitive unit cell consisting four atoms (Tl-Se-Bi-Se-) perpendicular to the threefold axis along [111] of cell. Analogous calculations have been done for  $\text{SnBiSe}_2$ ,  $\text{SbBiSe}_2$ ,  $\text{Bi}_2\text{Se}_2$ ,  $\text{TlSnSe}_2$  and  $\text{PbSbSe}_2$  [44]. Specifically, all of the materials have an even number of surface states along the (111) direction. Such materials are part of weak topological insulators (WTI). The interest in WTIs comes partially because their surface states are strongly protected from defects by the delocalization of the somewhat helical surface electrons.  $\text{GaBiSe}_2$  is proved to be a strong topological insulator (STI) since it has a single Dirac cone at the  $\Gamma$ -point on the surface.  $\text{PbBiSe}_2$ ,  $\text{SnBiSe}_2$ ,  $\text{SbBiSe}_2$ ,  $\text{Bi}_2\text{Se}_3$ ,  $\text{TlSnSe}_2$ ,  $\text{PbSbSe}_2$  etc., WTIs have an even number of surface states within the bulk band gap [43-45]. Another family of ternary chalcogenide is found to be showing topological behaviour in the ambient conditions as well. The electronic structures of  $\text{TlBiSe}_2$  and  $\text{TlBiTe}_2$  slabs with different surface terminations are performed with the aid of DFT [42]. On flat (polar) Se/Te or Tl-terminated surfaces, the presence of

trivial dangling bond having Dirac cone states in sharp contrast to ARPES experiments on  $\text{TlBiSe}_2$  and  $\text{TlBiTe}_2$  where no similar trivial state is found near the Fermi energy. Here, in the bulk band gap there is an isolated Dirac cone and the rough (nonpolar) surfaces along (111) removed trivial SS having equal numbers of Tl and Se (Te) atoms in the surface layer of  $\text{TlBiSe}_2$ ,  $\text{TlBiTe}_2$ . This result compares remarkably well with experimental outcome. In addition, the appearance of superconductivity in bulk  $\text{TlBiTe}_2$  under *p-type* doping and theoretically-predicted Rashba type nontrivial surface states implied that it could be a candidate for driving topological superconductivity [44].

### 1.2.3 Strain and hydrostatic pressure induced Topological phase transition:

By varying the strength of SOC we can turn normal insulators (NIs) into TIs. This process of transition from one topology to another is known as 'topological quantum phase transition' (TQPT) [46]. Typically, the strength of SOC is increased with the heavy elements carrying high atomic numbers and it can be tuned by chemical doping, or substitution. Non-topological insulators which possess a significant SOC shows TQPT in external parameters i.e. under pressure/strain, temperature, or electric fields modifying the bulk crystal symmetry, even if they cannot be classified as a TI at ambient condition [47]. It remains the best way to do this transformation, with respect to other external parameters, especially looking for an efficient and clean route of pressure.

Above the all parameters, the hydrostatic pressure and strain is an important parameter that can be used to precisely control the effective hybridization, bond lengths (distances), volume, electron density, lattice parameters and crystal field splitting of materials [48]. It maintains the charge neutrality in the system. They have a very pronounced effect on the electronic band structure by reducing the band gap and derive BI by enhancing the strength of SOC. Consequently, for certain 3D NIs having small SOC the crucial electron behaviour characteristic of 3D TIs can be electronically accessed in response to applied higher pressure. The essential physics underlying this pressure-induced TQPT is the reduction, collapse or re-opening of band gap in certain materials which has weak SOC with applied external pressure. In the room pressure range, their band gap is too large to allow for a band inversion (BI) [46]. But at higher pressures, the band gap is reduced and Dirac point emerges as shown in Fig. 1.7 and the material shows non trivial behaviour. In the last decade, a lot of theoretical and experimental efforts have been devoted by condensed-matter physicists to uncovering the TQPTs induced pressure. This is particularly relevant in last decades because high-pressure

and strain induced TQPT has led to the momentous discovery of a significant enhancement of thermoelectricity that demonstrates how crucial this subject can be for society [43].

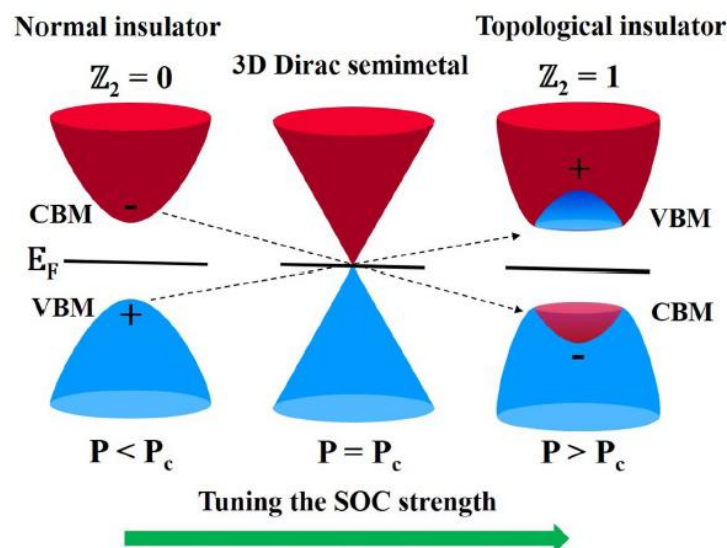


Fig. 1.8. Schematic diagram of Band structure at different hydrostatic pressure. [49]

#### 1.2.4 Topological Phase Transition in TlBiS<sub>2</sub> and TlSbS<sub>2</sub> using strain and hydrostatic pressure:

It was reported that many TI-based III-V-VI can be tuned into TIs from normal insulator with the help of pressure and strain. Using first-principles calculations TlBiS<sub>2</sub> and TlSbS<sub>2</sub> studied under the effect of pressure and strain. The first theoretical prediction of a phase transition under strain was for HgTe, which sparked great interest in the field of topological insulators and catalyzed many experimental efforts that eventually led to proof of concept experiments [50-51]. The strain induced topological phase transition has also been explored in various studies and shows the versatility of this approach to tune the electronic structure as desired topology.

TlBiS<sub>2</sub> and TlSbS<sub>2</sub> belong to ternary chalcogenide family having rhombohedral unit cell and  $R\bar{3}m$  space group. From fig. 1.9 below it can be seen that at ambient condition TlSbS<sub>2</sub> shows an energy gap of 0.128 eV at the  $\Gamma$ -points. Further increment on pressure (0-8GPa) the energy gap closes first closes and then reopens. At ambient conditions there is no BI occurs in the system shows topological trivial in nature. On 2 GPa at  $\Gamma$ -points the inverted contribution of Tl and S *p-orbital* shows in the conduction and valence band respectively; a BI occurs which signify the non-trivial nature of material. When we further increase the pressure even number of BI occurs at 5 GPa and the materials shows trivial in nature which can be further

verify with the help of parity analysis.  $\text{TlBiS}_2$  also displays topological property under the effect of hydrostatic pressure and strain [52].

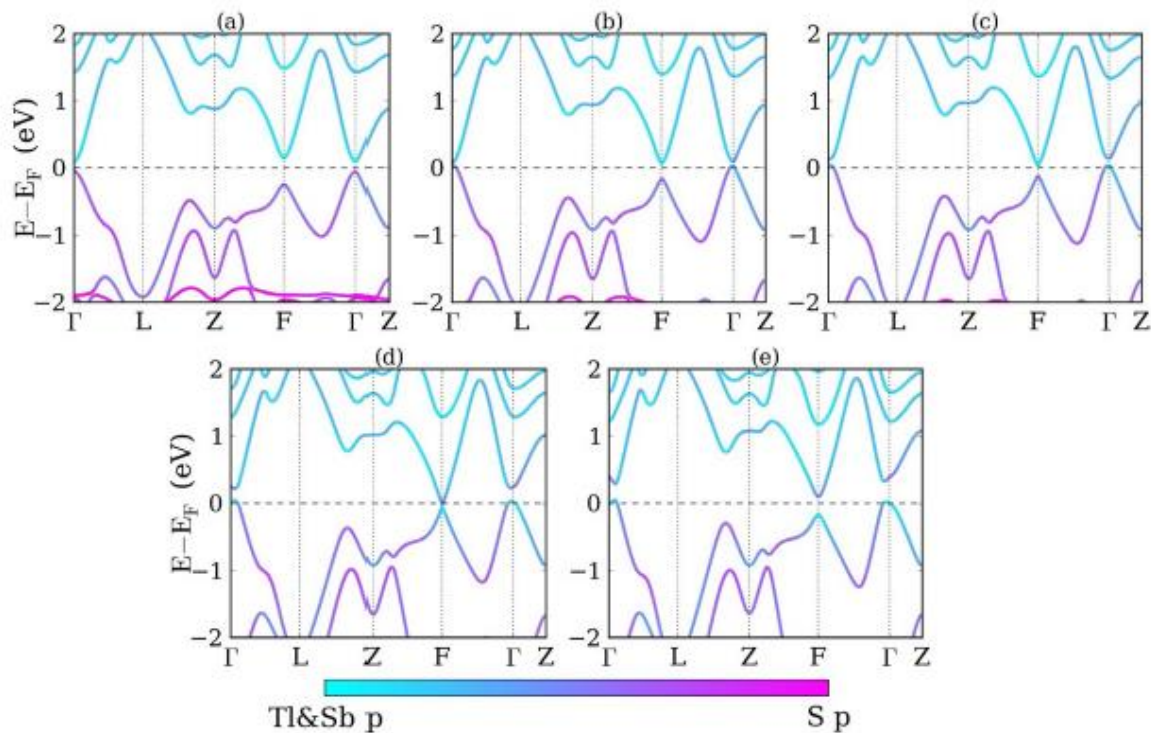


Fig. 1.9 band structure of  $\text{TlSbS}_2$  at (a) 0 GPa (b) 2 GPa (c) 3GPa (d) 5GPa (e) 8 GPa hydrostatic pressure [53].

### 1.2.5 Pressure induced TQPTs in rare-earth monpnictides family:

The rare-earth monpnictides  $\text{LnX}$  ( $\text{Ln}$  = a rare earth element;  $\text{X} = \text{As}, \text{Sb}, \text{Bi}$ ) a family of materials which has recently attracted great interest in scientific community. These compounds have shown very striking signatures of XMR (extremely large magnetoresistance) and superconductivity [54-55].  $\text{LaBi}$ ,  $\text{CeBi}$  also possessed topological properties and protected by SS [56]. Consequently, the existence of protected SS in these compounds implies that they might be suitable nodes for novel electronic effects-qualities which render them potentially useful to many other applications. This will allow insights into their electronic and magnetic properties that might help identify new materials with purpose-designed functionalities applicable in next-generation electronic devices and quantum technologies [48].  $\text{LaBi}$  [57],  $\text{LaSb}$  [58] and  $\text{LaAs}$  [55], surprisingly show giant magnetoresistance (XMR) effects which are ideal for sensor applications or even in spintronic devices. But the origin of these XMR in composites is still open to debate. Possible models include electron-hole-compensation or non-trivial band-topology.

It is reported that YbAs shows TQPT under the effect of hydrostatic pressure. By using first-principles calculations at ambient conditions this material shows trivial nature as shown in Fig. 1.10 below. When we increase the pressure at 6 GPa an BI can be observed at the  $X$ -point i.e. a small contribution of  $d$ -orbital of Yb in valence band and  $p$ -orbital of As in conduction band is found and the parities also switched at that point.

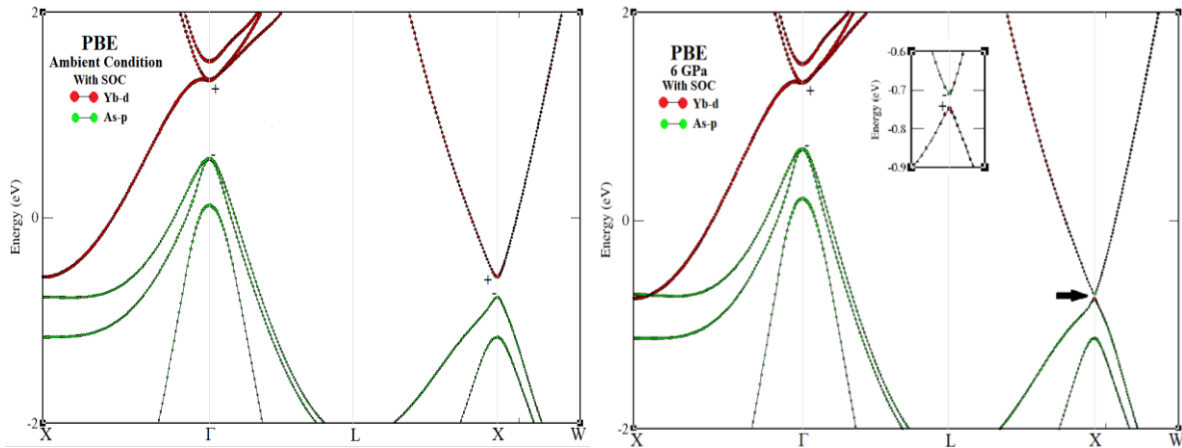


Fig. 1.10 Band structure of YbAs at (a) ambient pressure (b) 6 GPa hydrostatic pressure. [59]

The presence of Dirac cone in the surface states also confirms the non-trivial behaviour of material. YbAs shows topological behaviour till 39.5 GPa, after that the system returns to its initial state [59]. LaAs [55], LaSb [58], YBi [60] also shows topological behaviour under the influence of pressure.

## CHAPTER 2

### METHODOLOGY

#### 2.1 Many body problem

This chapter has covered the theoretical approach used to characterize the topological features of materials. To calculate topological invariants, crystalline solids must have an exact electronic structure. The precise electrical structure of solids can be obtained by solving the Schrödinger equation for a large number of particles. But a lot of particle wave functions comprise a large number of variables, making it hard to solve this Schrodinger equation. To understand the many body problem let us consider Schrodinger equation for this system [54]:

$$H \Psi (\mathbf{R}, \mathbf{r}) = E \Psi (\mathbf{R}, \mathbf{r}) \quad 2.1$$

Where ' $H$ ' represents the many-body Hamiltonian, ' $\Psi (\mathbf{R}, \mathbf{r})$ ' represents the wave function for the positions of nuclei ( $\mathbf{R}$ ) and electrons ( $\mathbf{r}$ ), respectively, corresponding to an energy eigen value ' $E$ '. On ignoring the relativistic effects, Hamiltonian for such a system is difficult to solve. Here the situation is more complicated because many electrons are interacting with multiple nuclei. So several approximations are taken to solve many body problem and density functional theory comes (DFT) in picture [61].

#### 2.2 Density Functional Theory:

In the wave function-based approach, the many-body wave function relies on the coordinates of all electrons within a system. For a system containing ' $N$ ' electrons, the wave function involves ' $4N$ ' variables, accounting for the three-dimensional spatial coordinates and spin coordinates for each electron. This comprehensive dependence on individual electron coordinates makes solving the Schrödinger equation exceedingly complex and computationally intensive [62].

To mitigate this complexity, Density Functional Theory (DFT) was introduced. DFT reduces the problem by employing the electron density as a fundamental variable. The electron density represents the integral of the square of the wave function over all ' $N-1$ ' electrons. Each spin density of a system becomes a function of only three spatial coordinates, regardless of the system's size. The utilization of density as a variable in solving the many-body problem is the core principle of DFT. This approach revolutionized computational quantum mechanics

by simplifying calculations and making them more feasible for larger systems. In recognition of their pivotal contributions to this field, Walter Kohn and John Pople were awarded the Nobel Prize in Chemistry in 1998 for their work on Density Functional Theory [63].

The Hohenberg-Kohn theorem states that the ground-state electronic density uniquely determines the ground-state wave function of a many-electron system, and vice versa, for a given external potential. This theorem essentially asserts that all observable properties of an interacting many-electron system can be expressed as functional of the electronic density.

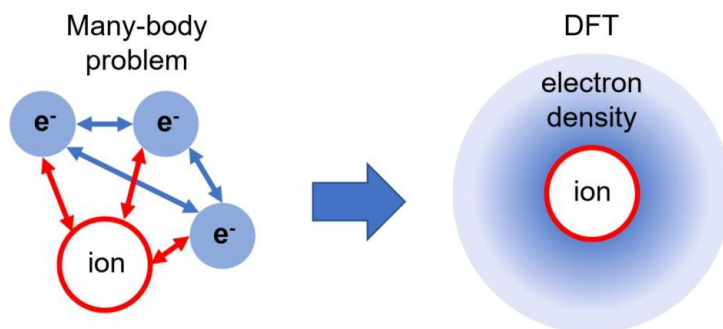


Fig.2.1. The representation of the theme of Density functional theory [63].

The Hohenberg-Kohn theorem highlights a crucial aspect of the functional; The electron density that minimizes the overall functional energy corresponds to the true electron density associated with the complete solution of the Schrödinger equation. If we were acquainted with the accurate functional form, we could iteratively adjust the electron density until the functional's energy is minimized, providing a method for determining the pertinent electron density. In practice, we apply the variational principle using approximate functional forms. Using the Born-Oppenheimer approximation, the nuclei of the treated molecules or clusters are taken to be stationary, creating a static external potential  $V$  in which the electrons are travelling. Then, a wavefunction  $\Psi(\mathbf{r}_1, \dots, \mathbf{r}_N)$  meeting the many-electron time-independent Schrödinger equation can be used to describe a stationary electronic state.

$$\begin{aligned}
 \hat{H} \Psi &= [\hat{T} + \hat{V}_{nu-e} + \hat{V}_{e-e}] \Psi \\
 &= [\sum_{i=1,2,\dots,N} ((-\hbar^2/2m_i) \nabla_i^2) + \sum_{i=1,2,\dots,N} (V_{nu-e}(\mathbf{r}_i)) + \sum_{i<j} V_{e-e}(\mathbf{r}_i, \mathbf{r}_j)] \Psi \\
 &= E \Psi
 \end{aligned} \tag{2.2}$$

Where, for the system of  $N$  electrons,  $\hat{H}$  (Hamiltonian operator),  $E$  denotes the overall energy,  $\hat{T}$  denotes the kinetic energy operator,  $\hat{V}_{nu-e}$  denotes the potential energy operator corresponding to the external field due to the positively charged nuclei and  $\hat{V}_{e-e}$  denotes the operator corresponding to inter-electronic interactions. The operators  $\hat{T}$  and  $\hat{V}_{e-e}$  are identical for any  $N$ -electron system and for this reason, are called universal operators. The operator  $\hat{V}_{nu-e}$  depends on the specifics of a particular system. Owing to the inter-electronic interaction

term corresponding to  $\hat{V}_{e-e}$ , this many-particle equation is not separable into one-particle equations.

The application of DFT allows to map the many-particle problem, containing  $\hat{V}_{e-e}$ , to a one-particle problem free from  $\hat{V}_{e-e}$ . The electron density  $n(\mathbf{r})$ , a crucial quantity in DFT, is given for a normalized  $\Psi$  by

$$n(\mathbf{r}) = N \int d^3r_2 \dots \int d^3r_N \Psi^*(\mathbf{r}, \mathbf{r}_2, \dots, \mathbf{r}_N) \Psi(\mathbf{r}, \mathbf{r}_2, \dots, \mathbf{r}_N). \quad (2.3)$$

$$\Psi_0 = \Psi[n_0], \quad (2.4)$$

The fact that the wave function is a functional of  $n_0(\mathbf{r})$  immediately leads to the finding that the expectation value of an observable  $\hat{O}$  when the system is in the ground state is also a functional of  $n_0(\mathbf{r})$

$$O[n_0] = \langle \Psi[n_0] | \hat{O} | \Psi[n_0] \rangle \quad (2.5)$$

Further, it is possible to explicitly write the contributions due to the external potential

$\langle \Psi[n_0] | \hat{V}_{nu-e} | \Psi[n_0] \rangle$  as:

$$V_{nu-e}[n_0] = \int V_{nu-e}(\mathbf{r}) n_0(\mathbf{r}) d^3r \quad (2.6)$$

This argument can be extended and the contribution due to the external potential may be expressed as:

$$V_{nu-e}[n] = \int V_{nu-e}(\mathbf{r}) n(\mathbf{r}) d^3r \quad (2.7)$$

$T[n]$  and  $U[n]$  are referred to as universal functionals, but  $V_{nu-e}[n]$  being dependent on the specifics of the given system is referred to as a non-universal functional. Having specified a system, the minimization of the functional

$$E[n] = T[n] + V_{e-e}[n] + \int V_{nu-e}(\mathbf{r}) n(\mathbf{r}) d^3r \quad (2.8)$$

The objective is to minimize the energy functional concerning  $n(\mathbf{r})$ . The minimization process of the energy functional results in the determination of the ground-state electron density ( $n_0$ ), subsequently determining all other observables associated with the ground state.

The Lagrangian method of multipliers offers a solution to the variational problem of minimizing the energy functional  $E[n]$ . To initiate the process, we examine an energy functional that does not incorporate the inter-electronic interaction energy

$$E_{eq}[n] = \langle \Psi_{eq}[n] | \hat{T} + \hat{V}_{eq} | \Psi_{eq}[n] \rangle, \quad (2.9)$$

where  $\hat{T}$  denotes the operator corresponding to the kinetic energy, and  $\hat{V}_{eq}$  denotes the operator corresponding to the equivalent potential in which the particles are travelling.  $E_{eq}$  can be used to generate the following Kohn-Sham equations for this auxiliary, noninteracting system:

$$[-(\hbar^2/2m) \nabla^2 + V_{eq}(\mathbf{r})] \varphi_i(\mathbf{r}) = \varepsilon_i \varphi_i(\mathbf{r}), \quad (2.10)$$



which gives the orbitals  $\phi_i$  that mimic the electron density  $n(\mathbf{r})$  of the actual many-particle system

$$N(\mathbf{r}) = \sum_{i=1,2,\dots,n} |\phi_i(\mathbf{r})|^2. \quad (2.11)$$

The equivalent single-body potential may be expressed as

$$V_{eq}(\mathbf{r}) = V_{nu-e}(\mathbf{r}) + \int (n(\mathbf{r}')/|\mathbf{r}-\mathbf{r}'|) d^3r' + V_{EC}[n(\mathbf{r})], \quad (2.12)$$

Where the first term  $V_{nu-e}(\mathbf{r})$  is the extrinsic potential, the second term is the Hartree term expressing the inter-electronic Coulombic interaction, and the third term  $V_{EC}$  denotes the exchange-correlation potential. Here the entirety of the many-body interactions is incorporated in the exchange-correlation potential  $V_{EC}$ . The task of finding the solution to the Kohn-Sham equation is approached in an iterative self-consistent fashion. Initially, a starting guess for  $n(\mathbf{r})$  is made following which the corresponding  $V_{eq}$  is determined and the Kohn-Sham equations are solved for the  $\phi_i$ . Using these  $\phi_i$ 's a new electron density is determined and the aforementioned sequence of steps is repeated. Up until convergence, this process is repeated [63-64].

## 2.3 Exchange correlation functional

The actual form of the exchange-correlation functional, whose existence is guaranteed by the Hohenberg-Kohn theorem, remains unknown. However, there is a specific scenario in which we can precisely derive this functional: the uniform electron gas. In this instance, we assume that the electron density remains constant at all points in space. While this may seem limited in relevance to real materials, which exhibit variations in electron density defining chemical bonds and contributing to material properties, the uniform electron gas offers a practical means to apply the Kohn-Sham equations.

In this approach, we derive the exchange-correlation potential by setting it at each position to be the known exchange-correlation potential from the uniform electron gas at the electron density observed at that particular position. This is accomplished by analyzing the same system employed in the Kohn-Sham equations. Through the Kohn-Sham formulation of Density Functional Theory (DFT), the total energy is expressed as follows

$$E_{tot, KS-DFT} = - (1/2) \sum_i \int \Psi_i^*(\mathbf{r}) \nabla^2 \Psi_i(\mathbf{r}) d^3r - \sum_J \int (Z_J/|\mathbf{r}-\mathbf{R}_J|) n(\mathbf{r}) d^3r + \\ (1/2) \int \int (n(\mathbf{r}) n(\mathbf{r}')/|\mathbf{r}-\mathbf{r}'|) d^3r d^3r' + E_{EC} + (1/2) \sum_{I \neq J} ((Z_I Z_J)/|\mathbf{R}_I - \mathbf{R}_J|) \quad (2.13)$$

The first right-hand term side expresses the electronic non-interacting kinetic energy, the second term expresses the nuclei-electron interaction energy, the third term expresses the Coulombic inter-electronic interaction energy, the next term expresses the exchange-correlation energy and the fifth term expresses the inter-nuclei interaction energy. The

orbitals and the electron density  $n = \sum |\Psi_i|^2$  are attained by self-consistently solving the Kohn-Sham equations: Self consistently solving Kohn-Sham equations yields the orbitals  $\Psi_i$  and the electron density  $n = \sum |\Psi_i|^2$  that may be used for the determination of  $E_{tot, KS-DFT}$  :

$$(-\frac{1}{2})\nabla^2 - \sum_J (Z_J/|r-R_J|) + \int (n(r')/|r-r'|) d^3r' + v_{EC}(r)) \Psi_i(r) = \epsilon_i \Psi_i(r). \quad (2.14)$$

The exchange-correlation energy functional  $E_{EC}$  and potential  $v_{EC} = \delta E_{EC} / \delta n$  are the only terms in  $E_{tot, KS-DFT}$ , and the Kohn-Sham equations that are not precisely known. As a result, the correctness of the estimated characteristics is primarily dependent on the  $E_{EC}$  and  $v_{EC}$  estimates. A multitude of exchange and correlation approximations have been developed. They can be divided into several categories, including gradient approximation (GGA), local density approximation (LDA), meta-generalized gradient approximation (meta-GGA), and hybrid approximations [64].

## 2.4 Generalised Gradient Approximation:

When the exchange-correlation functional was expanded in terms of the gradient of the density through the Taylor series and terminated it at some order. Such an approximation is known as gradient expansion approximation (GEA) this was initiated by Herman in 1969 [65]. It turned out that such an approximation often gave worse results and did not provide any improvement over local density approximations. This was because the gradients of the density in real system become very large; as a result, such expansions break down. It was also found that the GEA does not satisfy most of the sum rules. Later only, it was realized that there was no need of such an expansion and it was possible to construct exchange—correlation functional, which was a functional of density as well as its gradient and satisfied the sum rules. This could be written as

$$E_{xc}[n_{\uparrow}, n_{\downarrow}] = \int d^2r f(n_{\uparrow}(r), n_{\downarrow}(r), \nabla n_{\uparrow}, \nabla n_{\downarrow}) \quad (2.15)$$

## 2.5 Perdew-Burke-Ernzerhof (PBE):

PBE is the relaxed generalized gradient approximation (GGA) proposed by Perdew-Burke-Ernzerhof and is one of the most often used exchange-correlation functional in DFT. PBE functionals improves on the local density approximation (LDA) by including gradient of the electron density in the calculation of exchange and correlation energies [66]. This functional has proven quite effective in modeling many materials properties covering a much broader spectrum of systems with higher accuracy than LDA, especially for molecular structures, surface energies, and some solids .

## **2.6 Modified Becke-Johnson (MBJ):**

MBJ is an improved exchange-correlation functional by Tran and Blaha, It is developed to address some of the shortcomings of conventional functionals for predicting band gaps, especially in semiconductors and insulators. The standard GGA or meta-GGA functional is corrected to more accurately represent the energies and electronic band gaps in MBJ. This functional has boasts greater accuracy in predicting band gaps for wide array of materials than the other functional, especially when the standard functional are not able to provide reasonable result [66].

## **2.7 Heyd-Scuseria-Ernzerhof (HSE):**

HSE06 is a hybrid functional which mix GGA with a portion of Hartree-Fock exchange. Heyd, Scuseria, and Ernzerhof proposed this to address the shortcomings described before with this method especially with materials with strongly correlated electrons or systems with significant charge transfer. The general hybrid meta-GGA functional employs a fraction of the exact exchange (as in HF theory) with the GGA exchange-correlation, to provide a more exact balancing of the description of both localized and delocalized electron behavior. The HSE06 hybrid functional is known to better describe properties such as band gaps, electronic structures of solids and materials with strong electron correlations, in a more accurate way than the pure GGA functional for certain systems [67].

## **2.8 Energy cut off:**

A new parameter cut off energy released to perform the DFT calculations. In most codes like VASP default cut-off energy is associated with every element in pseudo potential files i.e., ENMAX Therefore, although the energy is not explicitly defined, the calculation will employ the atom's pre-defined ENMAX. When calculating a system with more than one atom, the maximal ENMAX is considered by default. We define the Energy cut-off 1.3 ENMAX in the input of VASP to assure that the results will be stable and converged in all the above steps.

## **2.9 k-mesh sampling:**

One of the most crucial pieces of the band theory of solids is the Brillion Zone (BZ). In 1976 Monkhorst and Pack proposed a scheme to produce 'k' points special to specific irreducible Brillion Zone (IBZ). Its corresponding region in the reciprocal space is the IBZ that reproduces the full BZ with some symmetries. The IBZ has a number of advantages,

particularly for symmetric systems where it has a large reduction in computational effort when integrating over k-space. The usage of IBZ is to do the integrals in the smaller space (useful when your systems possess symmetries) such that typically much less work is needed to the computationally requirements. It is important to mention that the amount of computational time overall calculations depends on the number of 'k' points only inside the IBZ. However, the initial 'k'-point mesh should be carefully selected for getting better accuracy and convergence of the calculations. Thus, the convergence in the selection of the 'k' points is necessary to obtain accurate results from DFT calculations, which then affect the reliability and accuracy of the predicted properties [68].

## 2.10 $Z_2$ Topological Invariant:

To verify the topological phase transition in GdSb we computed the  $Z_2$  topological invariant using the product of parities at all TRIM points. In 3D as the system holds both inversion and TRS symmetry, there are four  $Z_2$  topological invariant  $\nu_0; (\nu_1\nu_2\nu_3)$  and the value of  $\nu_0$  can be calculated according to Kane and Mele criteria according to the following relation:

$$(-1)^{\nu_0} = \prod_{n_j=0,1} \delta_{n_1 n_2 n_3} \quad (2.16)$$

$$(-1)^{\nu_{i=1,2,3}} = \prod_{n_i=1; n_{j \neq i}=0,1} \delta_{n_1 n_2 n_3} \quad (2.17)$$

Here,  $\delta$  is representing the parities of all the filled occupied bands at TRIM points. The value of  $\nu_0 = 1$  corresponds to the topological phase transition in the system and  $\nu_0 = 0$  signifies the weak or trivial nature of the system. By determining the remaining three invariants we can identify the true nature of the system, if either of them comes to 1 then the system corresponds to weak topological insulator otherwise if all are zero tells the trivial nature of material [23].

## 2.11 Parity

Parity is defined as the reflection of a coordinate about origin. It is a transformation that flips the sign of one spatial- coordinate i.e.,  $\mathbf{x}$  to  $-\mathbf{x}$ . In quantum mechanics, the Parity operator, always commutes with the Hamiltonian if the potential is symmetric and therefore they have a common set of eigenstates.

$$P^\wedge |L, L_z\rangle = (-1)^l |L, L_z\rangle \quad (2.17)$$

Here,  $l$  is the orbital angular quantum number;  $L$  and  $L_z$  are the operators for the total angular orbital moment and its component in the  $z$  direction respectively. The orbital quantum number has the values of 0, 1, 2, 3.... for  $s, p, d, f$  orbitals respectively.

## 2.12 VASP

The Vienna Ab Initio Simulation Package, commonly referred to as VASP, is a tool employed for conducting ab initio quantum mechanical calculations. This involves the use of Vanderbilt pseudopotentials or the projector augmented wave method, coupled with a plane wave basis set. VASP solves the many-body Schrödinger equation approximately by solving the Kohn-Sham equations (in the framework of DFT) or by solving the equations (in the framework of the Hartree-Fock approach). Additionally, certain hybrid functionals that inherit aspects from both the Hartree-Fock approach and the DFT are also available. VASP calculates key quantities through plane wave basis: single-electron orbitals, charge density, and local potential. The interactions between the electrons and ions are either expressed with the help of the projector augmented wave method or with the help of norm-conserving or ultrasoft pseudopotentials [61]. The VASP code carry out calculations using 4 necessary input files, which are INCAR, POTCAR, POSCAR and KPOINTS.

## 2. 13 Phonopy package:

Phonon dispersion spectrum was shown to visualize the phonon frequencies by the Phonopy package to check the dynamical stability of the system. This is made using the harmonic and quasi harmonic approximation, where the atom in the crystal frame oscillates around the equilibrium positions. First, new equilibrium lattice constants (from VASP) were set and used to define the supercell (including symmetry of the system) using Phonopy. Using VASP finite-displacement method took advantage of this and was finally able to compute Force Constants for the new supercell. Phonopy was used to provide calculations of post-processing the dynamical matrix after extracting the force constants from VASP output. Then, using this dynamical matrix, we calculated the phonon frequencies at given  $q$ -points, resulting in a dynamical stability of the system.

## 2.14 Wannier90 packages:

This package Wannier90 was developed by Mosto et al. used in the tight-binding context for Wannier Functions (WFs) in the original Works of Wannier for tight-binding Hamiltonians in 2008

[61]. Finally, the MLWFs are used to determine several sophisticated electronic properties like Fermi surface, Berry Curvature and Anomalous Hall Conductivity in a more efficient and rigorous way. It should be emphasized that Wannier90 can only process VASP inputs produced through the VASP2WANNIER90 interface. Input flags in VASP to generate inputs for Wannier90. The use of VASP is well documented elsewhere. The basic usage of Wannier90 is mainly through four input files; **wannier.win**: a file holding the important information for the atomic coordinates and cell parameters. **wannier.mmn**: file provides the information on the bands (the same one as in wannier.win) and their overlaps. **wannier.amn**: In wannier.amn file the information is number of bands as pointed in wannier.win) and their projections. **wannier.eig**: The eig file is a file that contains Kohn-Sham (KS) eigenvalues (in eV), at each point in the Monkhorst-Pack k-mesh. These set of files work together to allow researchers to perform calculations and post-processing analysis on MLWFs, within materials, to explore complex electronic properties and states [69].

## CHAPTER 3

### The TPT in rare-earth monpnictide GdSb

#### 3.1 Abstract:

In our present work, we study the topological phase transition in rare-earth monpnictides GdSb using first principles calculations, under the influence of hydrostatic pressure. Likewise, all other materials of this family, it also crystallizes in rocksalt type *NaCl-crystal* structure for the entire study of pressure range. The structural phase transition occurs at 26.1 GPa and the material transforms into *CsCl-type* structure. The structural, electronic, and topological properties are studied using the hybrid density functional theory. At ambient conditions the material shows topological trivial in nature which is well matched with the experimental results. The topological phase transition is studied under the effect of external parameter pressure. The occurrence of BI inversion at 6 GPa shows the non-trivial topological behaviour of material. The presence of Dirac cone along the surface state confirms the topological behaviour of material. Moreover,  $Z_2$  topological invariant is also calculated for investigating the true nature of material using the product of parities at TRIM. When we further increase the pressure the material shows another band inversion near the Fermi level at  $\Gamma$  as well as X points. The GdSb shows its trivial state at 12 GPa as confirmed by the even no. of Dirac cone in the surface state. The zero values of first  $Z_2$  topological invariant confirms that the system returns back to its initial state.

We examined the GdSb material in the current work, which belongs to a member of the rare earth monpnictides family, and we experimentally validated that it is a trivial topological semimetal in nature at ambient condition. It is well known that rare earth monpnictides shown interesting behaviour topologic properties and superconductivity under the effect of strain and pressure. GdSb has been reported to show non trivial topology under the effect of strain, yet there is no theoretical investigation of topological behaviour of material with the effect of pressure. These theoretical and experimental investigations provide a feasible way to study the topological behaviour GdSb with an external hydrostatic pressure. The topological states are observed having an inversion of band in the electronic structure which can be further confirmed by calculating the  $Z_2$  topological invariant by calculating the product of parities at time reversal invariant point with various pressure ranges. The surface Dirac cone is projected for confirming the nature of different surface state.

### 3.2 Computational details:

Within the context of PAW, as implemented in the VASP, first principles calculations are carried out to examine the structural and electrical properties of material at different pressures using density functional theory. The structural optimization are performed GGA) [65] of PBE [66] until forces are smaller than 0.001 eV. The exchange correlations energy are calculated using GGA-PBE as well as HSE06 For the plane wave basis placed in the electronic structure, the total cut off energy of 240 eV is employed. All calculations take into consideration the influence of SOC, with the exception of ionic optimization, and the overall energies converge to  $10^{-6}$  eV. For sampling the Brillouin zone in rocksalt primitive unit cell  $7 \times 7 \times 7$  k-mesh is used. The system's enthalpy is computed using GGA within a pressure range of 0-27 GPa, whereas the band structure computations are executed within a pressure range of 0-12 GPa. The dynamical stability of the material is confirmed by phonon calculations by performing the phonon dispersion curve using the PHONOPY code [69] under various pressure range. By employing the product of parities at TRIM locations, the  $Z_2$  topological invariants were calculated in accordance with the Kane and Mele criteria [23].

### 3.3 Results and discussions:

Similarly to other rare earth monpnictides, GdSb similarly crystallizes in a *NaCl-type* rocksalt crystal structure at ambient conditions. Its space group is  $Fm\bar{3}m$  and its atomic positions are (0, 0, 0) for Sb and (0.5, 0.5, 0.5) for Gd, as illustrated in Fig. 3.1 (a). Our optimized lattice parameter is 6.248 Å which is consistent with experimental reports.

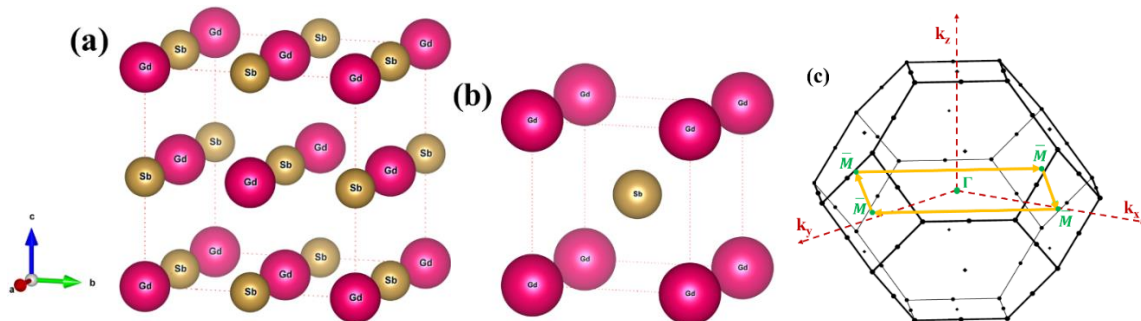


Fig.3.1. Crystal structure of GdSb (a) *NaCl-type* (b) *CsCl-type* (c) The BZ of GdSb with (001) plane (yellow color).



At high volumetric pressures the crystal structures convert from *NaCl* to *CsCl*-type showing structural phase transition (SPT). The enthalpy of both crystal structures at 0-27 GPa has been determined in order to make sure its SPT. The stability of structure having lower enthalpy  $H = E + PV$  (where  $E$  denotes the total energy,  $P =$  pressure and  $V =$  volume of the unit cell) at a given pressure is more stable. At ambient pressure *NaCl* has more stable than *CsCl* which lies lower to the *CsCl* curve as shown in Fig.3.2 (a). When we increase the pressure the enthalpy of both structures increases as defined in above equation and crossover at 26.1 GPa showing that *CsCl* is more stable at that pressure, which is known as transition pressure in Fig.3.2 (b). Moreover, phonon dispersion at various applied pressures using the Phonopy code verifies the material's dynamic stability. At ambient condition the material is dynamical stable as confirmed by the lack of negative frequency as shown in the Fig. 2(c). Furthermore, we have also checked its dynamical stability at pressure 26.1 GPa and we can say that the material is also stable at this pressure range illustrated in Fig.3.2 (d).

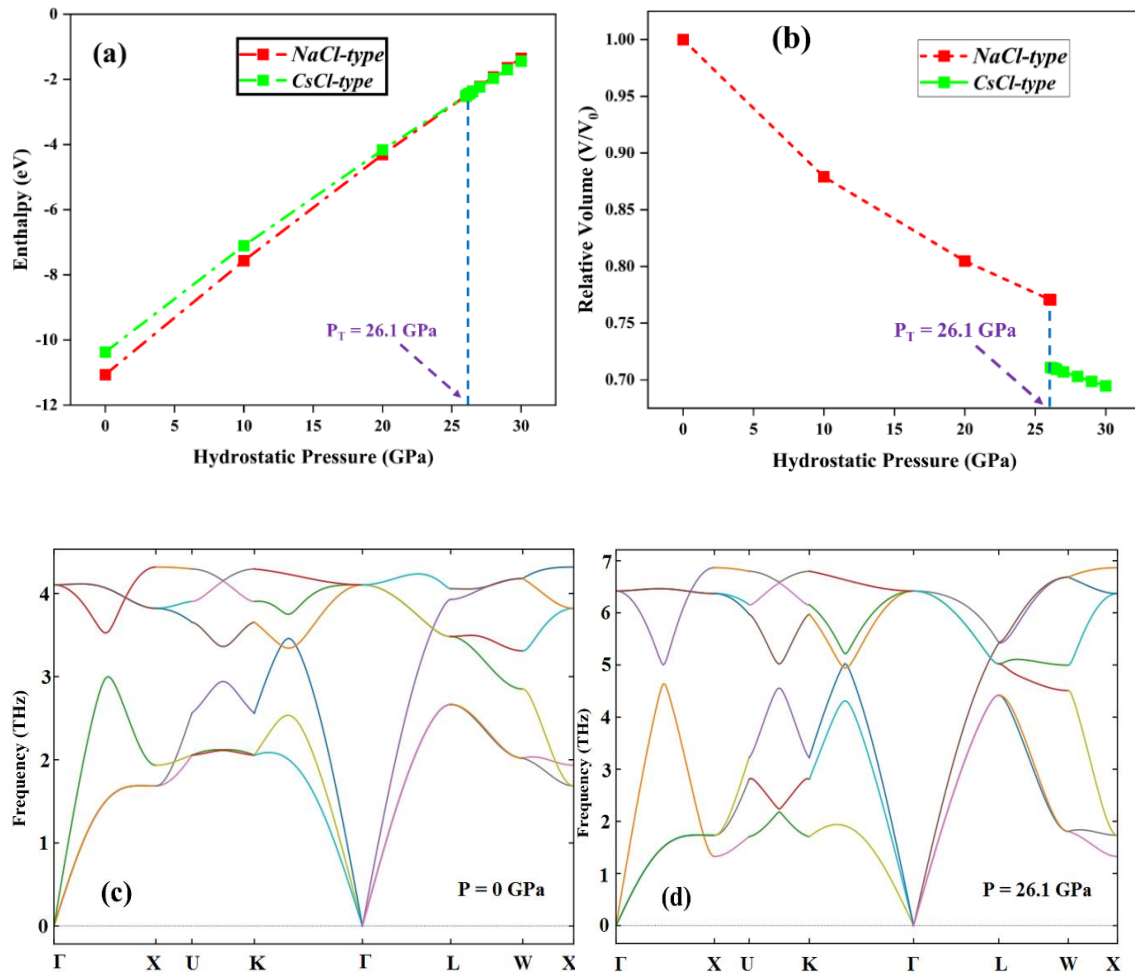


Fig.3.2. (a) Enthalpy of GdSb as function of pressure for *NaCl*-type to *CsCl*-type structure. (b) Variation in relative volume of GdSb as a function of pressure. The phonon dispersion of GdSb at (c) 0 GPa, (d) 26.1 GPa.

After determining the stability of crystal structure, we investigate true nature of material calculating their band structures at ambient conditions using two functional GGA-PBE and HSE06. Band structure plotting is done along the high symmetric points  $X$  to  $\Gamma$ ,  $\Gamma$  to  $L$ ,  $L$  to  $X$ ,  $X$  to  $W$  because it contains TRIM points in the BZ. From Fig. 3.3 (b) at ambient condition using PBE there is an overlapping of band occurred at  $X$  and  $\Gamma$  points. The valence band has mainly contribution from the Sb  $p$ -orbital and conduction band has mainly contribution from Gd  $d$  orbital. The even number of band inversion signifies the topological semimetallic nature of material. On the other hand, using HSE06 there is an energy gap occurs at ambient condition illustrated in Fig. 3.3 (c). Near the Fermi level the  $p$ -orbital of Sb and  $d$ -orbital of Gd are mainly contributed. The lack of band inversion is consistent of the material's topological triviality, which is consistent with our observations. The lack of Dirac cone in surface state also confirms the trivial nature of material as shown in Fig. 3.3 (d). Hence, we can say that we predict the true state of material at ambient conditions.

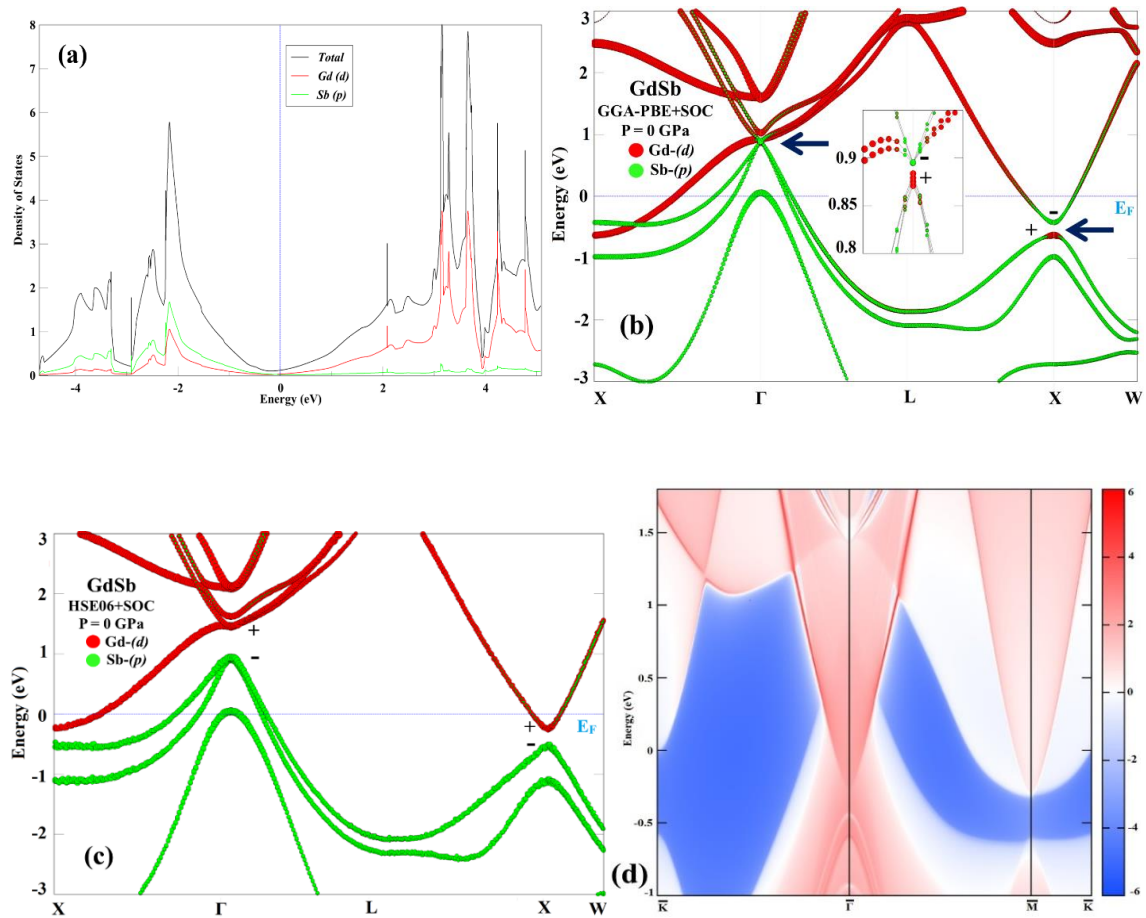


Fig. 3.3. The band structure of GdSb with inclusion of SOC effect using (a) GGA-PBE, (b) Projected density of states (c) HSE06 (d) The surface state. The Fermi level is set to 0 eV.

We examine the electronic band structure in the pressure range of 0–12 GPa to investigate the topological phase transition in material under hydrostatic pressure. It is widely recognized that the PBE functional can produce unphysical band structure predictions when pressure increases; therefore to determine the accurate nature of material we used HSE06 for our further calculations. From Fig. 3.4 (a) it can be seen that at 6 GPa there is a contribution of Sb *p-orbitals* and Gd *d-orbitals* in the conduction and valence band respectively. The inverted contribution in the electronic band structure creates an inversion of band at *X-point* which is the primary signature of non-trivial topological behaviour of material. The topological phase transition also verified by calculating surface state of the material. The presence of Dirac cone along the (001) shown in Fig. 3.4 (b) plane confirms the non-trivial behaviour of GdSb.

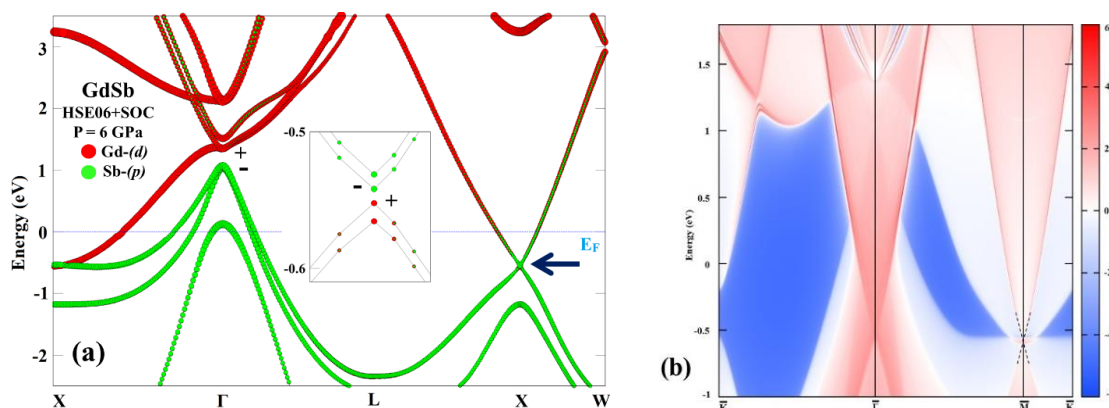


Fig. 3.4. (a) Band structure of GdSb with the inclusion of SOC effect using HSE06 functional at 6 GPa. (b) The surface state. The Fermi level is set to be 0 eV.

The system remains its topological state up to 11 GPa. When we further increase the pressure another band inversion occurs at Y points as shown in Fig 3.5 (a). The even number of band inversion corresponds to either weak or trivial nature of material which can be further ensuring by calculating their  $Z_2$  topological invariant. Two Dirac cones are seen in the bulk band structure at a certain position in the projection of the surface Brillouin zone, as shown in Fig. 3.5 (b-c). This observation validates the trivial nature of the material.

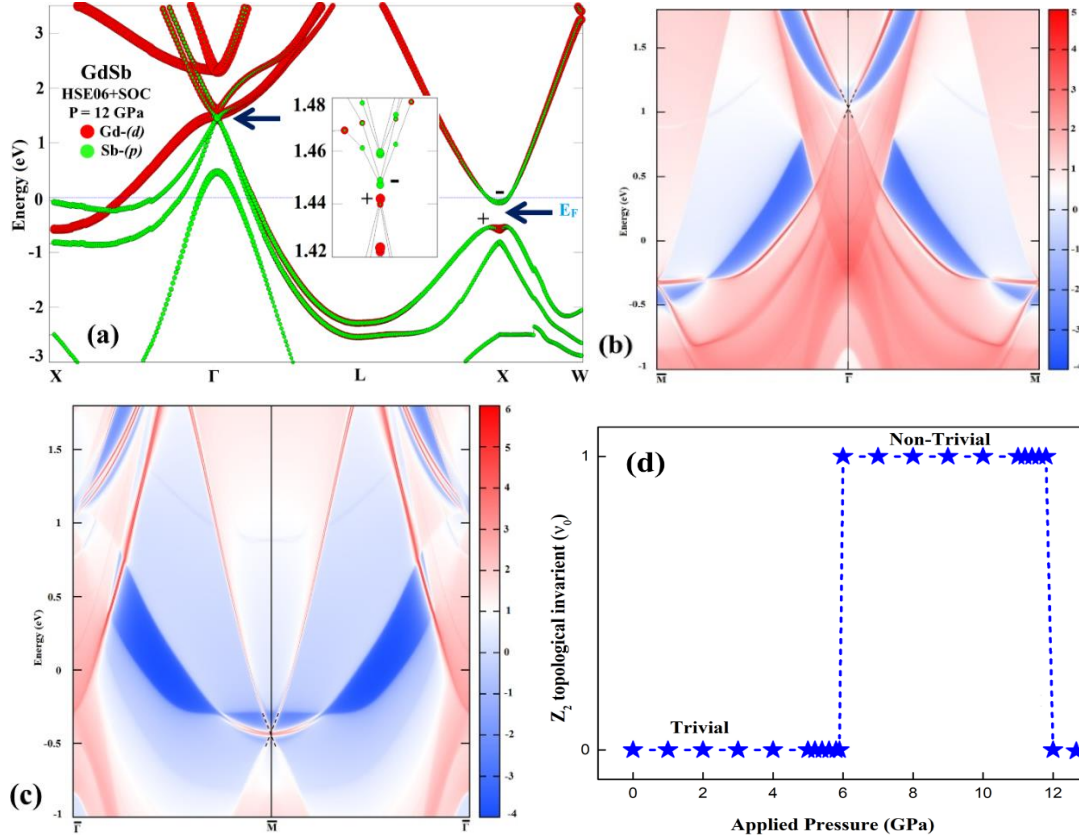


Fig. 3.5. (a) Band structure of GdSb with the inclusion of SOC effect using HSE06 functional at 12 GPa. (b, c) The surface state. The Fermi level is set to be 0 eV.

### 3.4 $Z_2$ topological invariants

The parities of material under the various pressure ranges are described in Table 3.1 as shown below:

Table 3.1: The parities at all TRIM points in BZ at various pressure range.

Hydrostatic Pressure	No. of band inversion	3X	4L	$\Gamma$	$Z_2$ invariants
0 GPa	No inversion	-	+	-	(0;000)
6 GPa	One inversion	+	+	-	(0;000)
12 GPa	Even no. of inversion	-	+	-	(1;000)

At ambient condition using PBE the system shows an even no. of band inversion the electronic band structure which shows the semimetal behaviour of material. Furthermore, the topological behaviour of material is confirmed by the value of first  $Z_2$  topological invariant. From the table it can be seen that the value of  $\nu_0$  comes to be 0 which confirms the topological trivial nature of material also agree with the experimental results, so we predict the true nature of material at ambient condition. When we increase the pressure the at 6 GPa

an band inversion occurs in the system that shows the non trivial topology. The parity of the highest occupied band at  $X$ -point switched and hence product of parities changes from positive to negative. The change in product of parities, switch first  $Z_2$  topological invariant from zero to one (according to equation 2.16) which confirms the non-trivial topological phase in the system. Furthermore, when we increase the pressure up to 12 GPa, a second inversion in bulk band structure is observed at  $\Gamma$ -point and hence parity of highest occupied band at this point switched. This change in parity affect the product of parities and it becomes positive again. The positive product of parities of all occupied bands concludes first  $Z_2$  topological invariant ( $v_0$ ) to be zero again. The first  $Z_2$  topological invariant is zero and even number of band inversions can direct the system either weak or trivial topological nature. This can be decided by remaining three topological invariants which follows the equation 1. The value of ( $v_1v_2v_3$ ) comes out to be zero confirms that the system returns backto its trivial state. The Fig. 4 (d) shows that how the values of first  $Z_2$  topological invariant changes with the effect of pressure.

### 3.5 Conclusion:

We have systematically investigated the structural, electrical, and topological properties of the material utilizing first principles methods using hybrid functional (HSE06) and GGA-PBE under the influence of hydrostatic pressure. At first, we have checked the structural stability of the material and finds that a structural phase transition occurs at 26.1 GPa the system transforms from  $NaCl$  to  $CsCl$  type crystal structure. The dynamical stability of material is verified with the help of phonon dispersion curve. The lack of negative frequency confirms the dynamical stability of material under various pressure ranges. At ambient condition the system shows topological trivial nature and matched with the experimental results. The trivial behaviour of material is also confirmed by the lack of Dirac cone and first  $Z_2$  topological invariant. The topological phase transition in GdSb is studied under the external pressure. At 6 GPa a single band inversion occurs in the electronic band structure shows non trivial topological nature. The parities switched at  $X$ -point and the non-zero value of  $Z_2$  invariant verify the non trivial state of material. The presence of Dirac cone confirms topological behavior of the material. On further increases the pressure an even no. of band inversion occurs at the  $X$ - as well as  $\Gamma$ -points and the system return to its initial state. The even number of Dirac cone establishes the trivial nature of GdSb which is further verified by the zero value of  $Z_2$  topological invariant.

## CHAPTER 4

### ***A first-principles study of strain-driven structural, dynamical, and topological properties of novel Sn-based ternary chalcogenide SnPbSe<sub>2</sub>***

#### **4.1 Abstract:**

As mentioned in the preceding aspects, there is a strong need of isolated Dirac cone in the  $A_2B_3$  compounds because in these type of system there is a flow of electron from bulk to surface state. Therefore, the topological properties are breaks. Following the isostructural substitution we have studied the topological phase of ternary chalcogenide  $SnPbSe_2$  using *first-principles* calculation. Here, we have reported a topological phase transition in  $SnPbSe_2$  under the effect of biaxial strain. The structural optimization, dynamical stability and electronic structure properties are analyzed and a topological band inversion is observed at 2% of biaxial strain. The  $Z_2$  topological invariants are calculated with the help of the product of parities of all the occupied wave functions at TRIM points. This topological phase transition provides an ideal platform for further experimental work.

#### **4.2 Computational details**

The DFT [63] based electronic structure calculations were performed within the PAW [] method as implemented in the VASP [67]. The structural optimization was performed using GGA with the help of PBE functional. The Fermi level broadening was done using the Gaussian smearing method and set at a width of 0.001eV. The exchange and correlation energy were calculated with the help of GGA-PBE as well as mBJ [64] functionals. The effect of SOC is included in all calculations except in ionic optimization and the total energies are converged to  $10^{-6}$  eV. A plane-wave cut-off energy and optimized Monkhorst-Pack type k-mesh of 320 eV and  $7 \times 7 \times 4$ , respectively were used. The phonon calculations of  $SnPbSe_2$  were performed using the PHONOPY code [68]. The  $Z_2$  topological invariants were computed using the product of parities at TRIM points as per the Kane and Mele model [23].

#### **4.3 Results and discussion**

The material  $SnPbSe_2$  belongs to the III-V-VI<sub>2</sub> TI-based family having a rhombohedral crystal structure with space group  $R\bar{3}m$  (166). The optimized lattice parameters for rhombohedral structure are  $a=b=4.343 \text{ \AA}$  and  $c=21.262 \text{ \AA}$ . This material can be realized as a sequence of hexagonally closed packed layers in the order Sn-Se-Pb-Se, where Pb and Sn layers are

sandwiched in the middle of Se layers as shown in Fig. 3.1(a). The primitive unit cell having four atoms is used to avoid band folding in the calculation of the bulk band structure as shown in Fig. 4.1(b). The crystal structure holds inversion symmetry where both Sn and Pb layers act as inversion centers that allow us to perform the calculation of the parities of the Bloch wave functions at the TRIM point.

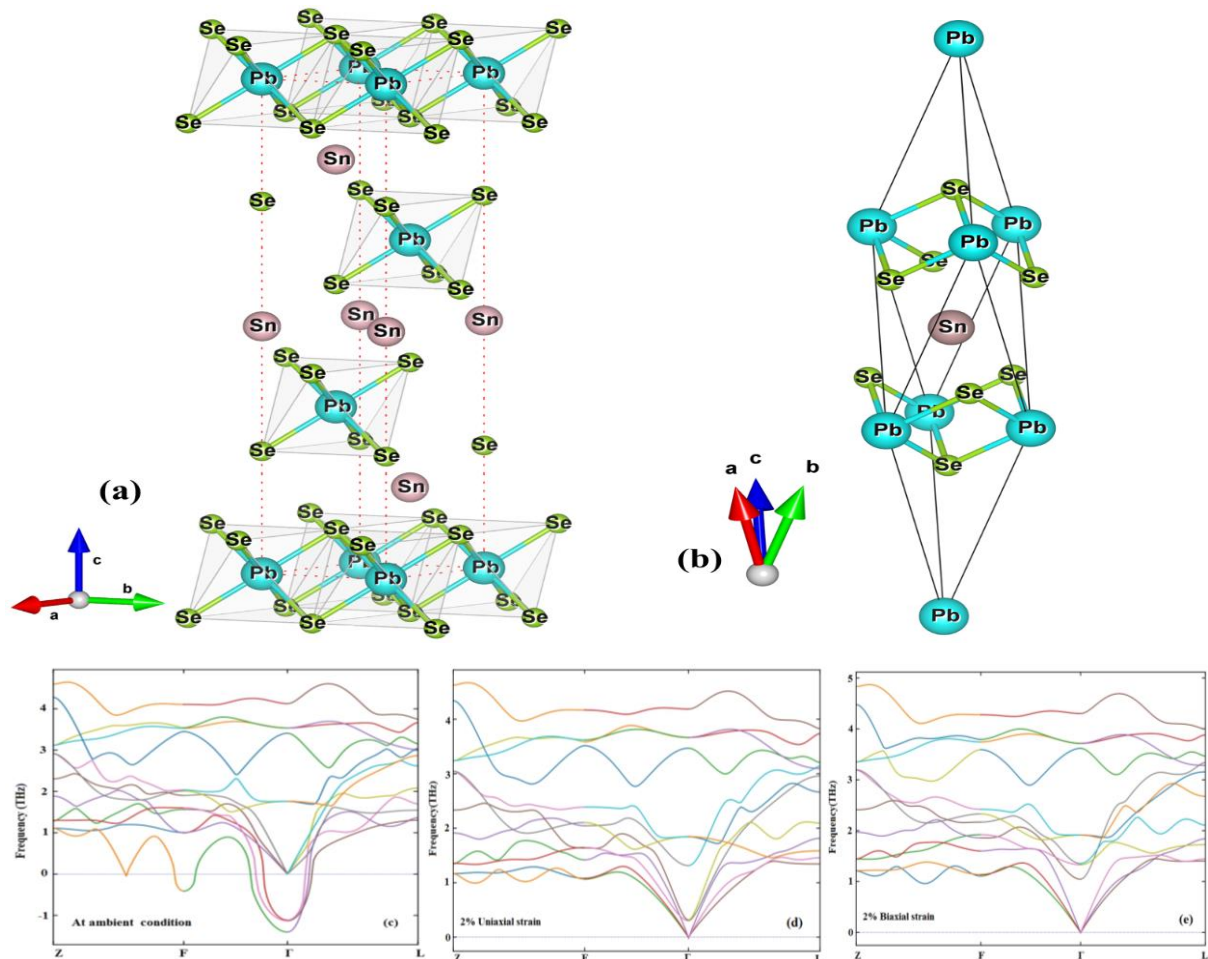


Fig.4.1. the crystal structure of SnPbSe<sub>2</sub> in (a) conventional unit cell (b) primitive unit cell. The phonon dispersion spectrums of SnPbSe<sub>2</sub> (c) at ambient condition and (d-e) applied 2% of uniaxial and biaxial strain.

Further, we analyzed the lattice dynamical stability of the SnPbSe<sub>2</sub> using phonon dispersion relation. At ambient conditions, this material shows negative frequencies that lead to the unstability of the material as shown in Fig.4.1(c). However, a small uniaxial stain along the c-axis or biaxial strain along equal lattice parameters reduces the negative frequency and increases the dynamical stability of the material. We observed that 2% of both uniaxial and biaxial strain makes this material dynamically stable with no negative frequency observed as shown in Fig. 4.1(d-e).

To identify the ground state electronic nature of SnPbSe<sub>2</sub> at ambient conditions, we have calculated the bulk electronic band structure of this material using GGA-PBE functional with the effect of SOC. The band structure calculations are performed along the  $Z-F-\Gamma-L-Z$  momentum path in the irreducible Brillion zone which contains the eight TRIM points of the bulk material. It can be observed in Fig.4.2(a) that the  $p$ -orbitals of both Se and Pb mainly contributed to the valence band and the conduction band of this material near the Fermi level. An even number of band inversions near the Fermi level are observed which establishes the topological trivial nature of this material. Although, in general, it is observed that GGA-PBE underestimates the ground state of materials so we also analyze the ground state of material with more accurate functional i.e., TB-mBJ with inclusion of the effect of SOC. The TB-mBJ functional identified the true nature of the material and it was found that SnPbSe<sub>2</sub> shows a topologically trivial semiconductor nature Fig.4.2 (b) with a band gap of 0.136 eV.

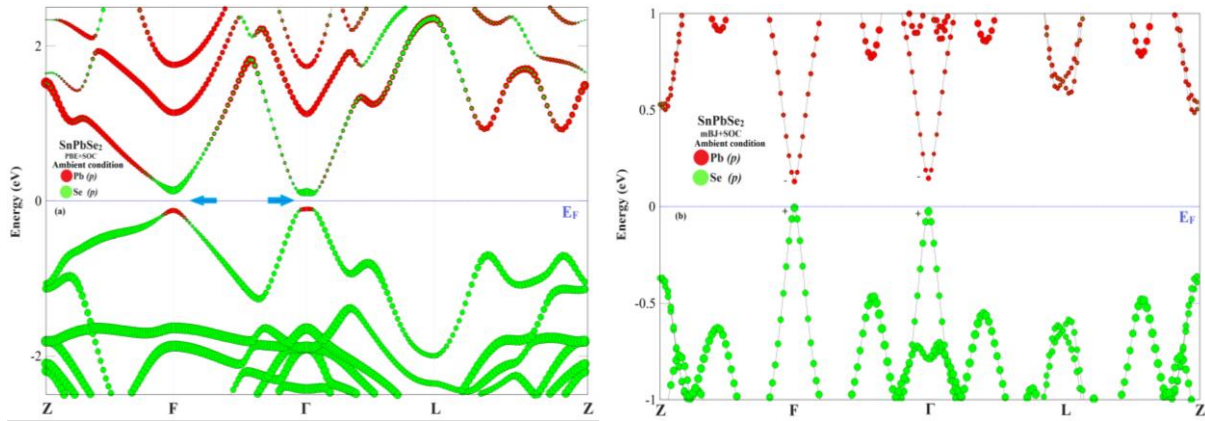


Fig.4.2. the electronic band structure of SnPbSe<sub>2</sub> at ambient condition using (a) PBE+SOC and (b) mBJ+SOC functionals. The Fermi energy is set to 0 eV.

To predict the topological phase transition, we have analyzed the bulk band structure of SnPbSe<sub>2</sub> under strained conditions. When we implemented the uniaxial strain along the  $c$ -axis of the material, no bulk band inversion was observed within the limit of experimental evidence of strain in materials []. However, we apply the 2% biaxial stain along the equal lattice parameter directions, a bulk band inversion is observed Fig. 4.3(a) at  $F$ -point. It should be noted that this material shows dynamical stability at above mentioned strained condition. An inverted contribution Fig. 4.3(a) of the  $p$ -orbital of Pb and  $p$ -orbital of Se in the valance and conduction band, respectively, established the above claim. At this condition, a reduction in the energy gap between the valance and conduction band at the  $\Gamma$ -point is also observed but band there is no band inversion. When we further increase the biaxial strain up to 3%, another band inversion at the  $\Gamma$ -point is also observed Fig. 4.3(b). Now, the inverted contribution of



the *p-orbital* of Pb and Se in the valance and conduction band, respectively, established an even number of bulk band inversion in this material at 3% biaxial stain. Now, this even number of band inversion shows that the system can be in the weak topological or topological trivial state, which should be further analyzed.

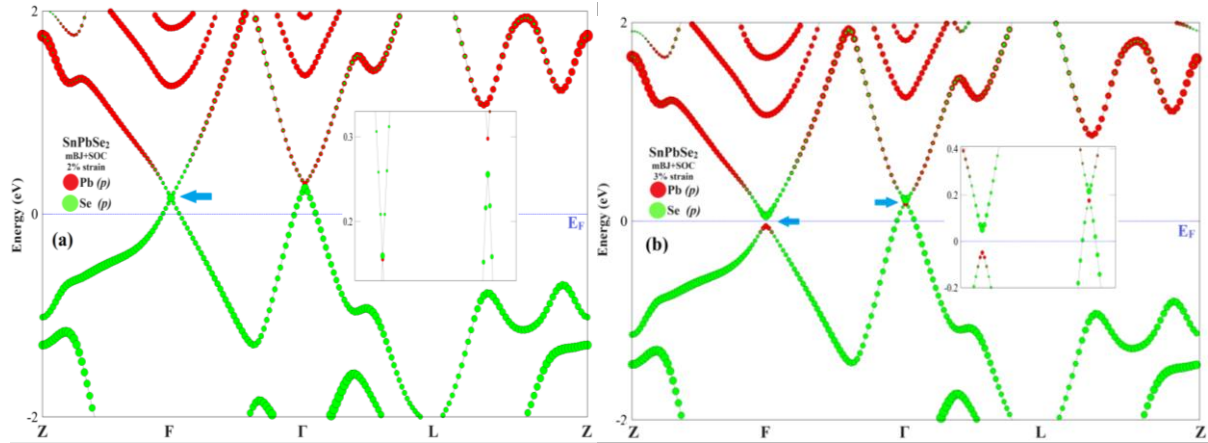


Fig.4.3. the electronic band structure of SnPbSe<sub>2</sub> using TB-mBJ functional (a) at 2% biaxial strain (b) at 3% biaxial strain. The Fermi energy is set to 0 eV.

## Z<sub>2</sub> topological invariant

To confirm the topological phase transition in SnPbSe<sub>2</sub> under the biaxial strain, we have calculated its Z<sub>2</sub> topological invariants at eight TRIM points. The product of parities at all TRIM points at different strained conditions is shown in Table 2. At ambient conditions, the product of parities is positive which shows that first Z<sub>2</sub> topological invariant  $\nu_0$  comes out to be 0 as calculated from equation 2.16. This observation verifies the topological trivial nature of the material observed in the bulk band structure. Under the condition of 2% biaxial strain the product of parities becomes negative and hence it changes the value of the first Z<sub>2</sub> topological invariant to 1 from 0. The non-zero value of the first Z<sub>2</sub> topological invariant established the non-trivial topological state of SnPbSe<sub>2</sub> at 2% biaxial stain. On further increasing the strain up to 3%, the product of parities becomes positive, and the first Z<sub>2</sub> topological invariant becomes 0. But, the even number of band inversions can study with the remaining three Z<sub>2</sub> topological invariants i.e., ( $\nu_1\nu_2\nu_3$ ). The product of parities calculated with different coplanar TRIM points is found to be positive. Hence all the remaining Z<sub>2</sub> topological invariants with positive product of parities (equation 2) become zero. This shows that the material becomes topologically trivial with an even number of band inversions observed in the bulk band structure. The variation of the first Z<sub>2</sub> invariant as a function of applied biaxial strain is represented in Fig. 4.4.

Table 4.1. The product of parities of all valance bands at TRIM points and  $Z_2$  invariants under conditions.

	<b>3Z</b>	<b>3F</b>	<b><math>\Gamma</math></b>	<b>L</b>	<b><math>Z_2</math> invariants</b>
GGA-PBE	+	-	-	+	(0;000)
TB-mBJ	+	+	+	+	(0;000)
2% Biaxial strain	+	-	+	+	(1;000)
3% biaxial strain	+	-	-	+	(0;000)

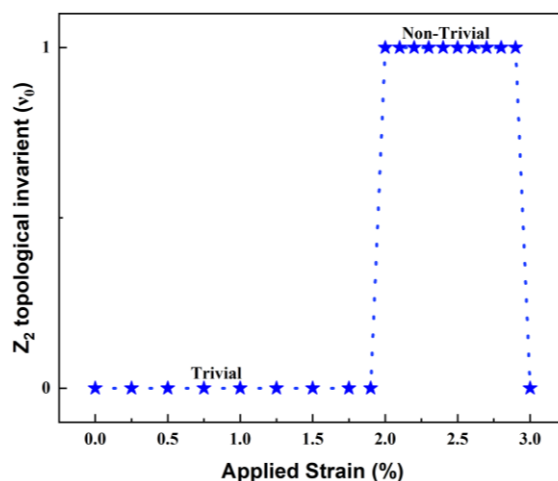


Fig.4.4. The first  $Z_2$  topological invariant ( $v_0$ ) as a function of applied biaxial strain.

## 4.4 Conclusion

Using a *first-principles* based approach, we have studied the structural, dynamical and topological properties of the ternary chalcogenide  $\text{SnPbSe}_2$  under applied uniaxial and biaxial strain. This material exists in a rhombohedral crystal structure with a topologically trivial semiconductor nature having an energy band gap of 0.136 eV. This material has shown dynamical instability at ambient conditions due to the existence of negative frequencies in the phonon dispersion relation. Under the applied uniaxial and biaxial 2% strain, this material becomes dynamically stable. At ambient conditions, this material has a topologically trivial nature with p-orbital of Sn and Pb mainly contributing near the Fermi level in the conduction and valance band, respectively. There is no topologically non-trivial nature observed with uniaxial strain along the c-axis. When we applied the 2% biaxial strain along the equal lattice direction of the material, a bulk band inversion at the *F-point* was observed and the material became topologically non-trivial. Further increase in biaxial strain up to 3% makes the system topologically trivial with an even number of band inversions. This topological phase transition from trivial to non-trivial and again from non-trivial to trivial with applied biaxial

strain has been verified with  $Z_2$  topological invariants. The zero and non-zero values of the first  $Z_2$  topological invariant are calculated with the help of the product of parities at all TRIM points corresponding to even and odd numbers of band inversions, respectively. This study confirms the topological phase transition in ternary chalcogenide  $\text{SnPbSe}_2$  with applied biaxial strain. The applied biaxial strain in this study is within the experimental framework observed in materials and can be utilized to guide a pathway for experimentally tuned topological properties in this material.

## REFERENCES

- [1] P. W. Anderson. Basic notions of condensed matter physics. CRC Press, 2018.
- [2] K. V. Klitzing, G. Dorda, and M. Pepper. New Method for High-Accuracy Determination of the Fine-Structure Constant Based on Quantized Hall Resistance. *Phys. Rev. Lett.*, 45:494 - 497, Aug 1980.
- [3] D. J. Thouless, M. Kohmoto, M. P. Nightingale, and M. den Nijs. Quantized Hall Conductance in a Two-Dimensional Periodic Potential. *Phys. Rev. Lett.*, 49:405-408, Aug 1982.
- [4] X.-L. Qi and S.-C. Zhang. The quantum spin hall effect and topological insulators. arXiv preprint arXiv:1001.1602, 2010.
- [5] M. I. Dyakonov and VI Perel. Current-induced spin orientation of electrons in semiconductors. *Phys. Lett. A*, 35(6):459, 1971.
- [6] M. König, S. Wiedmann, C. Brune, A. Roth, H. Buhmann, L. W. Molenkamp, X.-L. Qi, and S.-C. Zhang. Quantum spin Hall insulator state in HgTe quantum wells. *Science*, 318(5851):766{770, 2007.
- [7] J. E. Moore and L. Balents. Topological invariants of time-reversal-invariant band structures. *Phys. Rev. B*, 75:121306, Mar 2007.
- [8] X.-L. Qi and S.-C. Zhang. Topological insulators and superconductors. *Rev. Mod. Phys.*, 83:1057-1110, Oct 2011.
- [9] D. Hsieh, D. Qian, L. Wray, Y. Xia, Y. S. Hor, R. J. Cava, and M. Z. Hasan. A topological Dirac insulator in a quantum spin Hall phase. *Nature*, 452(7190): 970-974, 2008.
- [10] H. Zhang, C.-X. Liu, X.-L. Qi, X. Dai, Z. Fang, and S.-C. Zhang. Topological insulators in Bi<sub>2</sub>Se<sub>3</sub>, Bi<sub>2</sub>Te<sub>3</sub> and Sb<sub>2</sub>Te<sub>3</sub> with a single Dirac cone on the surface. *Nat. Phys.*, 5(6):438-442, 2009.
- [11] Nayak C., Simon S. H., Stern A., Freedman M., Sarma S. D.: Non-Abelian anyons and topological quantum computation *RMP* 80(3), 1083 (2008).
- [12] Yang S. A. Dirac and Weyl materials: fundamental aspects and some spintronics applications. *InSpin* (Vol. 6, No. 02, p. 1640003). World Scientific Publishing Company (2016).
- [13] Sangeeta, Kumar R., Singh M.: Realizing high thermoelectric performance in p-type RbZn<sub>4</sub>P<sub>3</sub> Zintl compound: a first-principles investigation *Journal of Materials Science J.Mater.Sci.* 57(23), 10691-701 (2022).

- [14] Rajamathi C. R., Gupta U., Kumar N., Yang H., Sun Y., Süß V., Shekhar C., Schmidt M., Blumtritt H., Werner P., Yan B.: Weyl semimetals as hydrogen evolution catalysts. *Advanced Materials* 29(19), 1606202 (2017).
- [15] K. Kuratowski. *Topology: Volume I, volume 1*. Elsevier, 2014.
- [16] M. Nakahara. *Geometry, topology, and physics*. CRC Press, 2003.
- [17] A. Bohm, A. Mostafazadeh, H. Koizumi, Q. Niu, and J. Zwanziger. *The geometric phase in quantum systems: foundations, mathematical concepts, and applications in molecular and condensed matter physics*. Springer Science & Business Media, 2013.
- [18] Budich, J. C. and Trauzettel, B. From the adiabatic theorem of quantum mechanics to topological states of matter. *Phys. Status Solidi RRL*, 7(1-2):109-129, 2013.
- [19] Kane C.L., Mele E. J.: Z<sub>2</sub> topological order and the quantum spin hall effect PRL 95, 146802 (2005).
- [20] Moore J. E.: The birth of topological insulators. *Nature* 464, 194 (2010).
- [21] Hasan M. Z, Moore J. E.: Three-dimensional topological insulators. *Annu. Rev. Condens. Matter Phys* 2(1), 55-78 (2011).
- [22] Hasan Zahid M., Neupane Xu. S. Y., M. Topological insulators, topological Dirac semimetals, topological crystalline insulators, and topological Kondo insulators. *Topological insulators: Fundamentals and perspectives*, 55-100 (2015).
- [23] Liang Fu., Kane C. L., Mele E. J.: Topological insulators in three dimensions PRL 98, 106803 (2007).
- [24] J. J. Sakurai and E. D. Commins. *Modern quantum mechanics, revised edition*. American Association of Physics Teachers, 1995.
- [25] R. J. Elliott. Spin-Orbit Coupling in Band Theory-Character Tables for Some "Double" Space Groups. *Phys. Rev.*, 96:280{287, Oct 1954.
- [26] P. Li and I. Appelbaum. Kramers' revenge. arXiv preprint arXiv:1801.10581, 2018.
- [27] A. A. Burkov. Topological semimetals. *Nat. Mater.*, 15(11):1145, 2016.
- [28] N. P. Armitage, E. J. Mele, and A. Vishwanath. Weyl and Dirac semimetals in three-dimensional solids. *Rev. Mod. Phys.*, 90:015001, Jan 2018.
- [29] X. Kong, L. Li, and F. M. Peeters. Topological Dirac semimetal phase in GexSny alloys. *Appl. Phys. Lett.*, 112(25):251601, 2018.
- [30] X. Huang, L. Zhao, Y. Long, P. Wang, D. Chen, Z. Yang, H. Liang, M. Xue, H. Weng, Z. Fang, X. Dai, and G. Chen. Observation of the Chiral-Anomaly-Induced Negative Magnetoresistance in 3D Weyl Semimetal TaAs. *Phys. Rev.X*, 5:031023, Aug 2015

- [31] M. M. Vazifeh and M. Franz. Electromagnetic response of Weyl semimetals. *Phys. Rev. Lett.*, 111(2):027201, 2013.
- [32] N. P. Armitage, E. J. Mele, and A. Vishwanath. Weyl and Dirac semimetals in three-dimensional solids. *Rev. Mod. Phys.*, 90:015001, Jan 2018.
- [33] A. Politano, G. Chiarello, B. Ghosh, K. Sadhukhan, C.-N. Kuo, C. S. Lue, V. Pellegrini, and A. Agarwal. 3D Dirac Plasmons in the Type-II Dirac Semimetal PtTe<sub>2</sub>. *Phys. Rev. Lett.*, 121:086804, Aug 2018.
- [34] R. K. Barik, R. Shinde, and A. K. Singh. Multiple triple-point fermions in Heusler compounds. *J. Phys.: Condens. Matter*, 30(37):375702, 2018.
- [36] R. K. Barik, R. Shinde, and A. K. Singh. Multiple triple-point fermions in Heusler compounds. *J. Phys.: Condens. Matter*, 30(37):375702, 2018.
- [37] A. A. Burkov, M. D. Hook, and L. Balents. Topological nodal semimetals. *Phys. Rev. B*, 84:235126, 2011.
- [38] M. Z. Hasan and C. L. Kane. Colloquium: Topological insulators. *Rev. Mod. Phys.*, 82:3045{3067, Nov 2010.
- [39] Zhang H., Liu C. X, Qi X. L, Dai X., Fang Z., Zhang S. C.: Topological insulators in Bi<sub>2</sub>Se<sub>3</sub>, Bi<sub>2</sub>Te<sub>3</sub> and Sb<sub>2</sub>Te<sub>3</sub> with a single Dirac cone on the surface. *Nature physics* 5(6), 438-42 (2009).
- [40] Yang J., Zheng B., Chen Z., Xu W., Wang R., Xu H.: Robust topological states in Bi<sub>2</sub>Se<sub>3</sub> against surface oxidation *J. Phys Sci.* 124(11), 6253-9(2020) .
- [41] Eremeev S. V., Bihlmayer G., Vergniory M., Koroteev Y. M., Menshchikova T. V., Henk J., Ernst A., Chulkov E. V.: Ab initio electronic structure of thallium-based topological insulators. *PRB* 83(20), 205129 (2011).
- [42] Singh B., Lin H., Prasad R., Bansil A.: Role of surface termination in realizing well-isolated topological surface states within the bulk band gap in TlBiSe<sub>2</sub> and TlBiTe<sub>2</sub>. *PRB* 93(8), 085113 (2016).
- [43] Lin, H., Markiewicz, R.S., Wray, L.A., Fu, L., Hasan, M.Z. and Bansil, A.: Single-Dirac-cone topological surface states in the TlBiSe<sub>2</sub> class of topological semiconductors *PRL* 105(3), 036404 (2010).
- [44] Phutela, A., Bhumla, P., Jain, M., & Bhattacharya, S. (2022). Exploring strong and weak topological states on isostructural substitutions in TlBiSe<sub>2</sub>. *Scientific Reports*, 12(1), 21970.
- [45] Duan X., Wu F., Chen J. Zhang., P. Liu. Y., Yuan. H. and Cao, C.: Tunable electronic structure and topological properties of LnPn (Ln= Ce, Pr, Sm, Gd, Yb; Pn= Sb, Bi). *Communications Physics* 1(1), 71 (2018).

- [46] Khalid S., Sabino F.P. and Janotti, A.: Topological phase transition in LaAs under pressure. PRB 98(22), 220102 (2018).
- [47] Guo P. J., Yang H. C., Liu K. and Lu. Z. Y.: Theoretical study of the pressure-induced topological phase transition in LaSb. PRB 96(8), 081112 (2017).
- [48] Barone P., Rauch T., Di Sante, Henk D., Mertig J., Picozzi. S.: Pressure-induced topological phase transitions in rocksalt chalcogenides. PRB 88(4), 045207 (2013).
- [49] Efthimiopoulos I., Kemichick J., Zhou X., Khare, S .V., Ikuta D. and Wang Y.: High-pressure studies of Bi<sub>2</sub>S<sub>3</sub>. J.Phys. Chem. 118(9), 1713-1720 (2014).
- [50] Yang M., Luo, Y. Z., Zeng M. G., Shen L., Lu. Y. H., Zhou J., Wang, S. J., Sou I. K. and Feng, Y.P., Pressure induced topological phase transition in layered Bi<sub>2</sub>S<sub>3</sub>. PCCP 19(43), 29372-29380 (2017).
- [51] Singh B., Lin H., Prasad R. and Bansil A.: Topological phase transition and quantum spin Hall state in TlBiS<sub>2</sub>. J.Appl. Phy. 116(3) (2014).
- [52] Zhang, Q., Cheng, Y., & Schwingenschlögl, U. (2015). Emergence of topological and topological crystalline phases in TlBiS<sub>2</sub> and TlSbS<sub>2</sub>. *Scientific reports*, 5(1), 8379.
- [53] X. Duan, F. Wu, J. Chen, P. Zhang, Y. Liu, H. Yuan, and C. Cao. Tunable electronic structure and topological properties of LnPn (Ln = Ce, Pr, Sm, Gd, Yb; Pn= Sb, Bi). Commun. Phys., 1(1):1{7, 2018.
- [54] A. Vashist, R. K. Gopal, D. Srivastava, M. Karppinen, and Y. Singh. Fermi surface topology and large magnetoresistance in the topological semimetal candidate PrBi. Phys. Rev. B, 99:245131, 2019.
- [55] R. Lou, B.-B. Fu, Q. N. Xu, P.-J. Guo, L.-Y. Kong, L.-K. Zeng, J.-Z. Ma, P. Richard, C. Fang, Y.-B. Huang, S.-S. Sun, Q. Wang, L. Wang, Y.-G. Shi, H. C. Lei, K. Liu, H. M. Weng, T. Qian, H. Ding, and S.-C. Wang. Evidence of topological insulator state in the semimetal LaBi. Phys. Rev. B, 95:115140, Mar 2017.
- [56] U. Dey. Comparative study of the compensated semi-metals LaBi and LuBi: first-principles approach. J. Phys.: Condens. Matter, 30(20):205501, 2018.
- [57] N. J. Ghimire, Y. Luo, M. Neupane, D. J. Williams, E. D. Bauer, and F. Ronning. Magnetotransport of single crystalline NbAs. J. Phys.: Condens. Matter, 27(15):152201, 2015.
- [58] Singh, M., Kumar, R., & Bibiyan, R. K. (2022). Pressure-induced topological phase transition in XMR material YbAs: a first-principles study. *The European Physical Journal Plus*, 137(5), 633.

- [59] Kumar R. and Singh M.: Topological phase transition and tunable surface states in YBi. arXiv preprint arXiv: 2309.05553 (2023).
- [60] I. N. Levine, D. H. Busch, and H. Shull. Quantum chemistry, volume 6. Pearson Prentice Hall Upper Saddle River, NJ, 2009.
- [61] W. Kohn. Nobel Lecture: Electronic structure of matter-wave functions and density functionals. *Rev. Mod. Phys.*, 71:1253{1266, Oct 1999. doi:10.1103/RevModPhys.71.1253.
- [62] J. A. Pople, P. M. W. Gill, and B. G. Johnson. Kohn|Sham density-functional theory within a \_nite basis set. *Chem. Phys. Lett.*, 199(6):557{560, 1992.
- [63] W. Kohn and L. J. Sham. Self-Consistent Equations Including Exchange and Correlation E\_ects. *Phys. Rev.*, 140: A1133{A1138, Nov 1965.
- [64] J. P. Perdew, K. Burke, and M. Ernzerhof. Generalized Gradient Approximation Made Simple. *Phys. Rev. Lett.*, 77:3865{3868, Oct 1996
- [65] A. D. Becke. A new mixing of Hartree Fock and local density-functional theories. *J. Chem. Phys.*, 98(2):1372{1377, 1993.
- [66] J. Heyd, G. E. Scuseria, and M. Ernzerhof. Hybrid functionals based on a screened Coulomb potential. *J. Chem. Phys.*, 118(18):8207{8215, 2003.
- [67] N. Marzari, D. Vanderbilt, and M. C. Payne. Ensemble Density-Functional Theory for Ab Initio Molecular Dynamics of Metals and Finite-Temperature Insulators. *Phys. Rev. Lett.*, 79:1337{1340, Aug 1997.
- [68] G. Kresse and J. Furthmuller. E\_iciency of ab-initio total energy calculations for metals and semiconductors using a plane-wave basis set. *Comput. Mater. Sci.*, 6(1):15{50, 1996.
- [69] N. Marzari, A. A. Mosto\_, J. R. Yates, I. Souza, and D. Vanderbilt. Maximally localized Wannier functions: Theory and applications. *Rev. Mod. Phys.*, 84: 1419{1475, Oct 2012. doi: 10.1103/RevModPhys.84.1419.





**DELHI TECHNOLOGICAL UNIVERSITY**  
(Formerly Delhi College of Engineering)  
Shahbad Daultpur, Main Bawana Road, Delhi-42

**PLAGIARISM VERIFICATION**

Title \_\_\_\_\_ of \_\_\_\_\_ the  
Thesis \_\_\_\_\_

\_\_\_\_\_ Total Pages \_\_\_\_\_ Name of the  
Scholar \_\_\_\_\_ Supervisor (s)

(1) \_\_\_\_\_

(2) \_\_\_\_\_

(3) \_\_\_\_\_

Department \_\_\_\_\_  
\_\_\_\_\_

This is to report that the above thesis was scanned for similarity detection. Process and outcome is given below:

Software used: \_\_\_\_\_ Similarity Index: \_\_\_\_\_, Total Word Count:  
\_\_\_\_\_

Date: \_\_\_\_\_

**Candidate's Signature**

**Signature of Supervisor(s)**

PAPER NAME

**thesis\_8\_plag.docx**

---

WORD COUNT

**10698 Words**

CHARACTER COUNT

**57386 Characters**

PAGE COUNT

**34 Pages**

FILE SIZE

**4.6MB**

SUBMISSION DATE

**Jun 6, 2024 2:01 PM GMT+5:30**

REPORT DATE

**Jun 6, 2024 2:02 PM GMT+5:30**

---

● **7% Overall Similarity**

The combined total of all matches, including overlapping sources, for each database.

- 5% Internet database
- 4% Publications database
- Crossref database
- Crossref Posted Content database
- 4% Submitted Works database

● **Excluded from Similarity Report**

- Bibliographic material
- Quoted material
- Cited material
- Small Matches (Less than 10 words)